Numerical Modeling of a Biomass Gasifier

MITACS-Vidir Internship Report

by

Jeremy Langner, M.Sc. Student

University of Manitoba
Faculty of Engineering
75A Chancellors Circle
Winnipeg, Manitoba, Canada
R3T 5V6

Feb 06th, 2008

Abstract

Biomass gasification is a thermo-chemical energy conversion process by which a solid organic fuel is converted to a combustible gas. The biomass fuel undergoes oxidation, pyrolysis, and reduction in an oxygen-starved environment at temperatures greater than 800 °C. The aim of the current project was to develop a 3-D numerical model of the primary gasification chamber in the Vidir two-stage gasifier-combustor, located at Arborg, MB. This 3-D model simulates the gasification of straw fuel in a fixed-bed gasifier by incorporating fluid mechanics, heat transfer, and chemical species transport and reaction mechanisms. Outputs from this model were compared with a zero-dimensional equilibrium gasification model, as well as available empirical data from the Arborg two-stage combustor. The peak temperature, outlet temperature, syngas composition, syngas heating value, and pressure drop were analyzed and compared for each of three cases – 25%, 50%, and 75% substoichiometric air. In general, the 3D model predicted higher outlet temperatures and lower syngas heating values than the equilibrium model. Syngas composition also varied significantly between the two models. Comparison with the empirical data was inhibited by flaws in the data; the most critical flaw was the high uncertainty in the measurement of the air supplied to the primary chamber. The absence of measurements of syngas composition prior to secondary combustion added to the difficulty of making this comparison.

Table of Contents

List of Figures

List of Tables

1.0 Introduction

1.1 Background

Today, most of the world's energy comes from non-renewable sources, specifically, oil, coal, natural gas, and nuclear [1]. However, as energy consumption increases at an ever-accelerating pace, as the price of oil continues to rise, and as the irreversible effects of climate change become increasingly apparent, the development and implementation of renewable energy sources is becoming an issue of paramount importance on the world stage. While hydropower is already firmly established, and wind, solar, and geothermal energy are growing, biomass energy is a resource with great potential for reducing dependence on fossil fuels and decreasing emissions of greenhouse gases worldwide. Biomass energy sources vary greatly in the types of fuel that can be used, and the methods of producing energy from these fuels. Biomass gasification is one such method.

Biomass gasification is fueled by organic matter; straw, switchgrass, reed grass, wood, cattails, and dried manure are several examples of possible candidates for gasification. Gasification occurs in an oxygen-deficient atmosphere at temperatures greater than 800°C [2c]. In an air or oxygen atmosphere, partial and complete oxidation reactions occur that provide heat to the system and consume the oxygen that is present. The elevated temperatures cause the pyrolysis of the solid fuel, releasing gaseous volatiles. Finally, reduction reactions such as the formation of methane and the water-gas shift reaction occur. A summary of the basic reactions is [2c]:

Partial oxidation:
$C(s) + 0.5O_2 \rightarrow CO$ $\Delta H = -268$ MJ/kmol (1)

Complete oxidation:
$C(s) + O_2 \rightarrow CO_2$ $\Delta H = -406$ MJ/kmol (2)

Water-gas reaction:
$C(s) + H2O \rightarrow CO + H_2$ $\Delta H = +118$ MJ/kmol (3)

Water-gas shift reaction:
$CO + H_2O \leftrightarrow CO_2 + H_2$ $\Delta H = -42$ MJ/kmol (4)

Methane formation:
$CO + 3H2 \leftrightarrow CH4 + H2O$ $\Delta H = -88$ MJ/kmol (5)

The product gas, called syngas, is composed largely of carbon monoxide, carbon dioxide, water vapour, hydrogen, and methane, as well as some larger hydrocarbons and tars. Since air is commonly used in the process instead of pure oxygen, a significant component of nitrogen is also present. The relative fractions of these components are largely based on the type of gasifier, as well as the amount of oxygen supplied. Typically, syngas heating values for gasification in air fall in the range of 4–6 MJ/m^3; in contrast, the higher heating value of natural gas is about 36 MJ/m^3 [2c].

Biomass gasifiers fall into two categories; fixed bed and fluidized bed gasifiers [3, 4]. Updraft, downdraft, and cross-flow gasifiers are common fixed-bed gasifiers. In an updraft gasifier, the biomass fuel is fed through the top of the chamber, while air is introduced from the bottom of the chamber [2c]. Thus, the flow of air and gas is opposite the motion of solid fuel. By contrast, the air and fuel flow in the same direction in a downdraft gasifier, reducing the amount of tar present in the syngas. In a cross-flow gasifier, the flow of air is perpendicular to the flow of fuel. Fluidized bed gasifiers use fine-grained bed material that forms a bed in which intimate mixing of the hot bed material, hot combustion gas, and biomass feed is achieved. An advantage of fluidized bed gasifiers is that a uniform temperature distribution can be established in the gasification zone. The circulating fluidized bed gasifier and the bubbling bed gasifier are two types of fluidized bed gasifiers.

1.2 Literature Review

Biomass gasification has been the focus of numerous studies in the recent past. McKendry [2a, 2b, 2c] provided a three-part review on biomass energy production, summarizing various types of biomass fuels and different conversion technologies. Biomass gasification was the subject of the third part of this review. Ruggiero and Manfrida [5] compared results from a steady-state equilibrium model of a gasifier against published experimental data. Zainal et al. [6] also used a steady-state equilibrium model to predict the performance of a biomass gasifier; the construction of this model is provided in detail. Matthieu and Dubuisson [7] developed a mathematical model that decoupled the processes of pyrolysis, combustion, the Boudouard reaction, and gasification; a sensitivity analysis was performed on several model parameters. Most recently, Zhou et al. [8] used a one-dimensional, transient, heterogeneous model to predict the advancement of the ignition flame front in a biomass gasifier.

1.3 Vidir Gasifier

The Vidir BEST Greenhouse Gas Displacement System is a biomass energy conversion system with the following components [9]:

1. Bale magazine for large, round bales
2. Bale shredder/conveyor system
3. Primary combustion chamber
4. Secondary combustion chamber
5. Hot water heat exchanger
6. Exhaust system
7. Computer control system

This system is designed primarily to use any fuel that is available in large, round bales, though other types of fuel can also be used. This system is displayed in Figure 1.

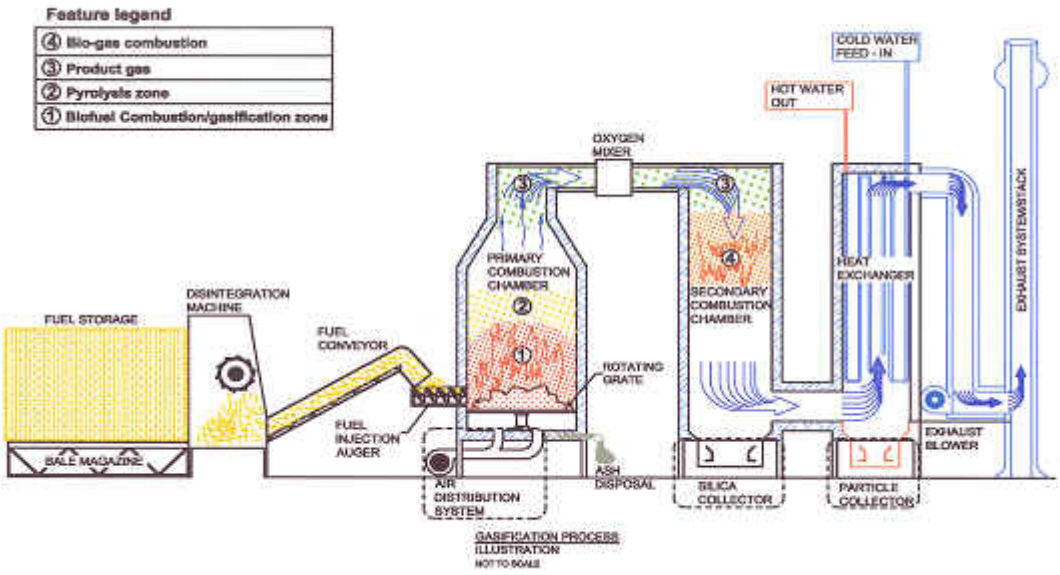

Figure 1: Diagram of the Vidir BEST Greenhouse Gas Displacement System

The focus of this project is the primary chamber, in which mainly pyrolysis and gasification reactions occur. Solid fuel is pushed into the primary chamber through a side fuel port using a ramming device. The fuel stacks up on a rotating grate, and as the fuel is consumed, the ash falls through the grate and is collected by the ash auger. Air is introduced to the primary chamber through inlets at the bottom of the chamber; instead of being blown in, the air is drawn in by a vacuum that is created in the chamber. The product gases, along with tars and partially combusted particles, rise up to the top of the chamber and are drawn into the secondary combustion chamber for further combustion.

The dimensions of the primary chamber at the BEST unit located at Arborg, MB were used for creating the geometry of the 3D model. For certain feature (such as the grate), the exact dimensions were unknown, so a reasonable approximation was used. In other cases (such as the air inlets), the geometry was simplified in order to curb model complexity. Figure 2 shows the dimensions used for the 3D model (all dimensions are in inches).

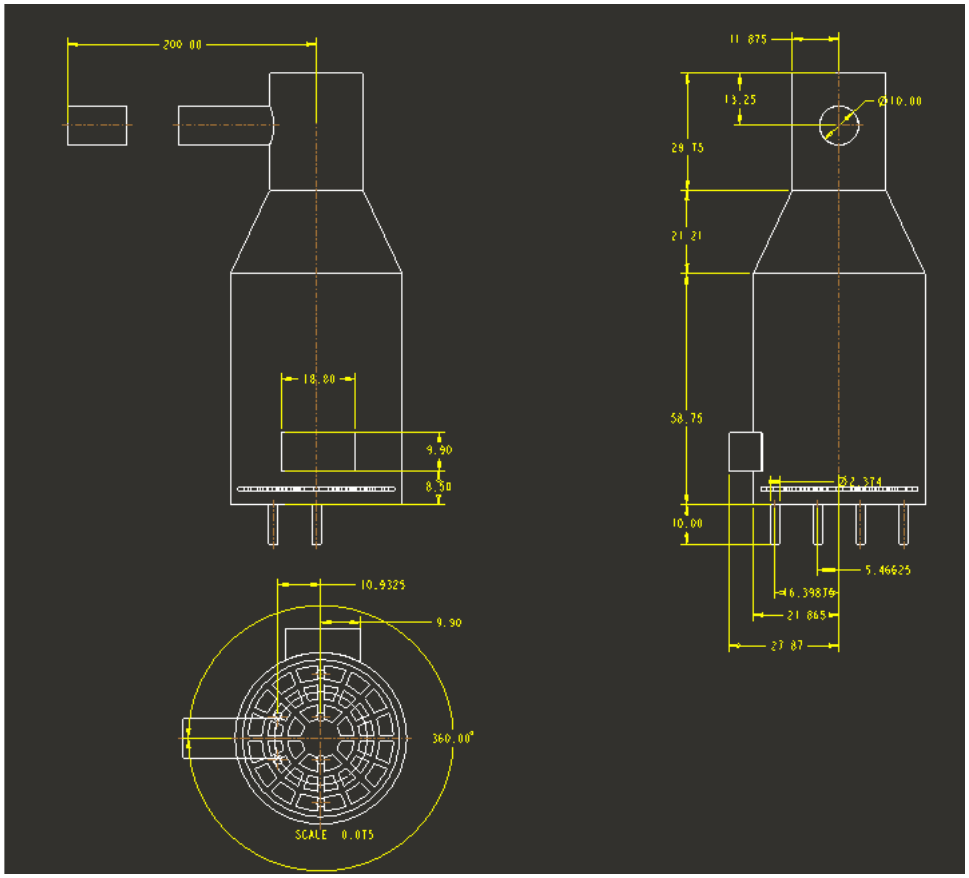

Figure 2: Primary chamber geometry used for the 3D model

2.0 Objectives

The aim of this research project was to develop a 3-D numerical model to simulate the gasification of straw within the primary chamber of the Vidir two-stage combustor located at Arborg, MB. This model was developed using Fluent [10] commercial CFD software. Specific objectives included:

Accurate prediction of 3-D fluid flow and heat transfer mechanisms. While zero- and one-dimensional gasification models are useful, they must assume uniform temperature and composition either throughout the entire gasifier chamber, or at each vertical location throughout the chamber. However, the chemical reactions involved in gasification can be very sensitive to local temperatures, species concentrations, and turbulent mixing conditions. Thus, an accurate 3-D model can predict how chemical species form and react locally within the chamber.

Effect of porous fuel bed. In the gasification chamber, a fixed bed of solid straw particles sits on top of a rotating grate. This straw bed has a significant impact on the fluid flow and heat transfer within the chamber. An aim of the current model was to simulate the effect of this fuel bed as a porous media with variable porosity.

Tracking of straw particles. Multiphase flow is an important consideration in the gasifier model; motion of both the gas phase and the solid straw particles must be taken into account, as well as interaction between gas and solid phases. This was done by tracking a representative number of straw particles using the Discrete Phase Model in Fluent.

Validation. Validation of the 3-D model was to be accomplished by comparison with empirical results from the Arborg two-stage combustor, as well as a zero-dimensional equilibrium model.

Incorporation into 3-D model of Vidir GHGDS. The current model is to be incorporated into a larger 3-D model that simulates the entire Greenhouse Gas Displacement System by Vidir Inc.

3.0 Zero-Dimensional Equilibrium Model

3.1 Overview

A zero-dimensional equilibrium model was constructed using the template of Zainal et al. [6]. This model makes the following assumptions:

1. All reactions are in thermodynamic equilibrium.
2. Species concentration and temperature are uniform throughout the chamber.
3. The gasifier chamber is perfectly insulated, with no heat transfer to the surroundings.
4. Air entering the chamber is dry (relative humidity is zero), with 23% oxygen and 77% nitrogen by mass.
5. Steady state operation is assumed.
6. The fuel may be represented by the chemical formula: CH_aO_b.
7. There is no differentiation between the volatile and char fractions within the fuel. It is assumed that solid fuel is entirely converted to gas, and all gas-phase reactants are allowed to come to equilibrium.

Two equilibrium reactions are modeled:

$$C + 2H_2 \leftrightarrow CH_4 \tag{6}$$

$$CO + H_2O \leftrightarrow CO_2 + H_2 \tag{7}$$

Thus, the overall gasification reaction may be described by:

$$CH_aO_b + wH_2O + m(O_2+3.76N_2) \rightarrow x_1H_2 + x_2CO + x_3CO_2 + x_4H_2O + x_5CH_4 + 3.76mN_2 \tag{8}$$

The model solves for product coefficients x_1 through x_5, and the molar air/fuel ratio m, using the equilibrium constant equations for both reactions, three mass balances (carbon, hydrogen, and oxygen), and the overall energy balance. This system of six equations and six unknowns is reduced to three non-linear equations and three unknowns via substitution, then solved iteratively using Newton's method for non-linear systems. A converged solution was generally easily obtained in under ten iterations.

The inputs for the model include:

- Fuel composition
- Fuel supply rate
- Initial temperature of fuel and air
- Reaction temperature
- Equilibrium constants for the gasification reactions
- Thermodynamic data for the chemical species involved - including enthalpy of formation H_f^0, Gibbs free energy G_f^0, and coefficients for specific heat C_p correlations.

The model outputs are:

- Air supply rate – dependent on the reaction temperature, the amount of air required to achieve this temperature was calculated.
- Syngas composition – the final gas composition reflects thermodynamic equilibrium.

3.1 Stoichiometric calculations

A stoichiometric calculation spreadsheet was also created to support and verify the equilibrium model. Inputs for this spreadsheet are: inlet temperature, air flow rate, fuel rate, and fuel composition (proximate and ultimate analysis). The syngas composition is determined by forcing the yields of CH_4 and H_2, then calculating the remaining components. A linear C_p model approximation is used so that a quadratic equation may be solved directly to find the outlet temperature. This spreadsheet may be easily used for verifying that the final syngas compositions predicted by either the equilibrium model or the 3-D model satisfy the appropriate mass and energy balances. A sample calculation is shown in Appendix A.

3.2 Volatile and fixed carbon components

From the point of view of an equilibrium model, no distinction needs to be drawn between what portion of the fuel is volatized, and what combusts as fixed carbon (char). However, this information is required for the 3-D model, where specific particles are tracked through the various stages of heating, vapourization, volatilization, and char combustion. Within the spreadsheet, the volatile composition is determined and represented as a molecule CH_xO_y. This volatile "molecule" must decompose into the product gases CO_2, CO, H_2, and CH_4 according to the reaction:

$$CH_xO_y \leftrightarrow aCO_2 + bCO + cH_2 + dCH_4 \quad (9)$$

For simplification, no tars or C_mH_n molecules are included in this decomposition.

4.0 Three-Dimensional Gasifier Model

4.1 Overview

The three-dimensional gasifier model is based on the geometry and operational conditions of the primary chamber of the Vidir two-stage combustor located at Arborg, MB. The following components of the model will be described in detail:

1. Geometry
2. Computational grid
3. Fluid dynamics and turbulence models
4. Heat transfer models
5. Porous media zone
6. Discrete phase model
7. Species transport and reaction model
8. Summary of cases studied

4.2 Geometry

The 3-D model is based on the primary chamber of the Vidir two-stage combustor. As shown in Figure 3, the main portion of the flow domain is a cylindrical chamber with a gradual flow contraction near the top. Six cylindrical air inlets are distributed around the bottom of the chamber. There are no inlets on one side of the chamber to allow room for an ash auger; the ash auger is not modeled here. A thick steel grate is located near the bottom of the chamber to support the biomass fuel bed. In reality, this grate rotates to mix the straw; this rotation was not incorporated into the model. A rectangular port on the side of the chamber allows for fuel to be rammed into the chamber. A horizontal outlet pipe extends from the top of the chamber. In reality, this outlet pipe is short and connects to a firing chamber where secondary air is added; this chamber is connected in turn to the secondary combustion chamber. Since only the primary chamber was considered, these are not a part of the model. The outlet pipe was extended in order to achieve fully developed flow at the outlet.

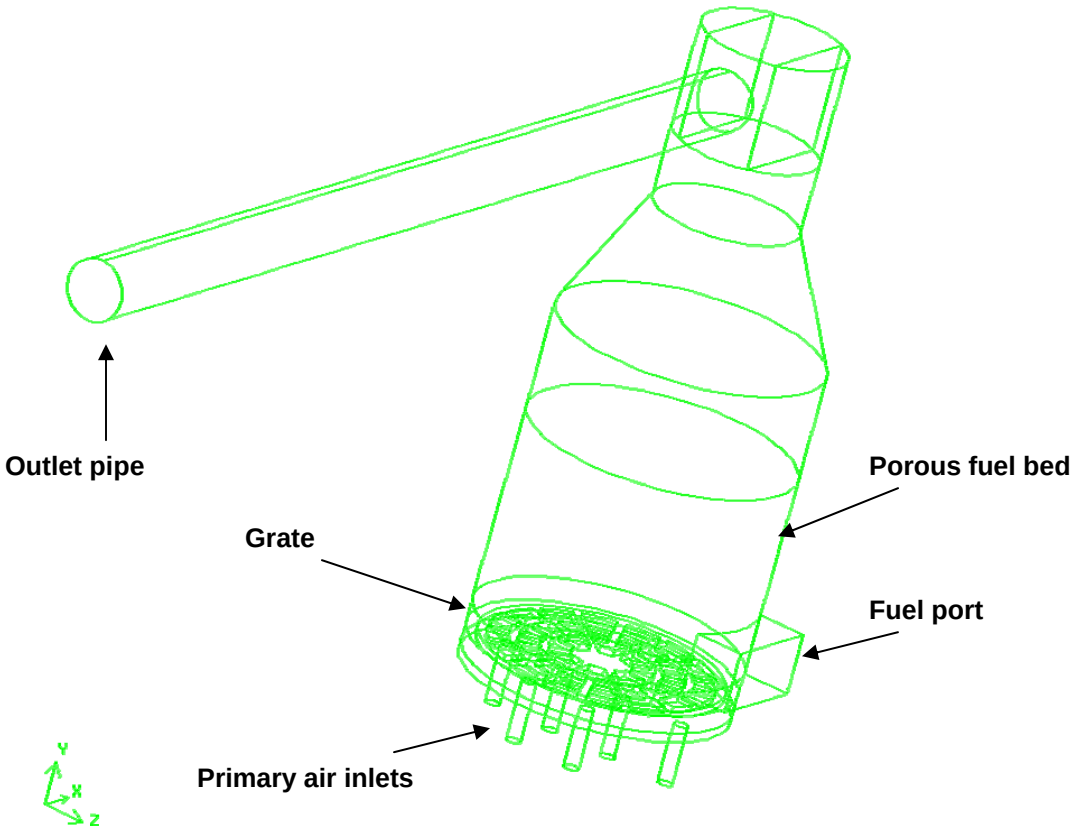

Figure 3: 3D geometry of the primary gasifier chamber

4.3 Computational grid

The domain geometry and the computational grid were generated using the GAMBIT [11] software package. The grid is a structured, hexahedral mesh, except for a small region around the grate in which an unstructured, tetrahedral mesh was used. The use of a structured, hexahedral mesh is beneficial, allowing for decreased computational time to achieve converged solutions. The grid used for the majority of model runs contained 182,675 elements. This is a relatively coarse grid; however, the complexity of the problem dictated that even so, fully converged solutions required on the order of 48 hours to achieve. A finer grid would increase this solution time even further. It was determined that fine resolution of the temperature, velocity, and turbulence fields was not required to achieve a suitable overall solution. No mesh refinement at the boundary layers was incorporated.

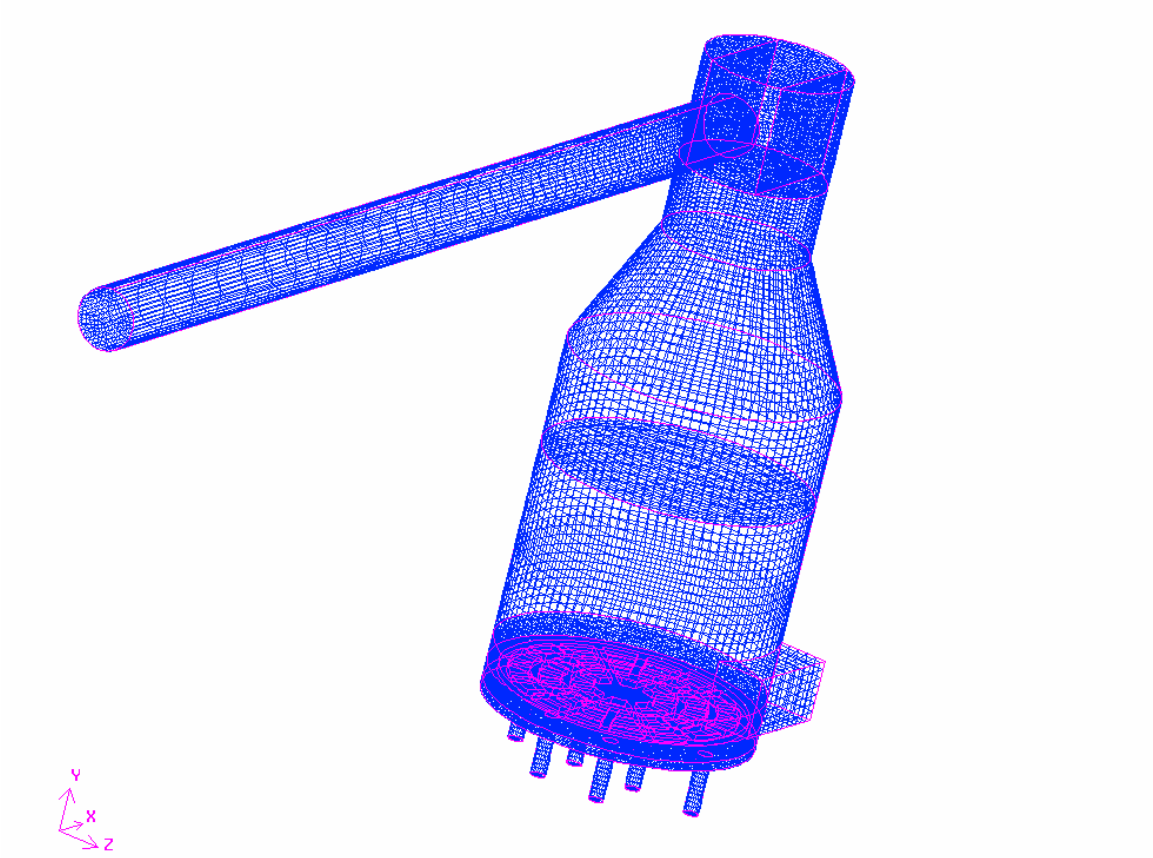

Figure 4: Computational grid for the 3D model

4.4 Fluid dynamics and turbulence models

Fluid flow within the 3D chamber was modeled under incompressible, steady state conditions. A segregated, cell-based, implicit solver was used to achieve the solution. The standard k-epsilon turbulence model with a standard wall function was employed.

The following flow boundary conditions were imposed:

- Inlets: Two separate mass flow inlet zones were defined. Six primary air inlets at the bottom of the chamber comprise the first zone, while the side fuel port was defined as a secondary air inlet. Air flow was split between the primary and secondary inlet zones according to a ratio of 5:3.
- Outlet: The exit of the outlet pipe was defined as an outlet
- Walls: All other surfaces within the domain were defined as walls, with a no-slip condition and a roughness coefficient of 0.5.

4.5 Heat transfer model

Energy transport and radiation equations were enabled to account for heat transfer throughout the chamber via conduction, convection, and radiation. The P1 radiation

model was used. The specific heat of each component gas was represented by a piecewise polynomial function.

The following energy boundary conditions were applied:

- Inlets: An inlet temperature of 320 K was set for both air inlets.
- Walls: An insulated (heat flux = 0) boundary condition was set on all walls. Surface emissivity was set at 0.5 for all walls.

4.6 Porous media zone

To simulate the effect of a packed bed of straw, a porous media zone was defined in the bottom half of the chamber. The porous media material was set as "straw". A user-defined function (UDF) was written to create a linear distribution of porosity as a function of radial position. Thus, porosity increases with distance from the centre of the bed. This was done in order to simulate the effect of molten biomass in the "hot zone" in the centre of the fuel bed. No direct measurements were possible to determine the actual porosity at the centre of the fuel bed.

4.7 Discrete phase model

The combustion of straw fuel was incorporated into the model using discrete combusting particles. Particle properties were defined according to the physical and thermal properties of straw (ie. size, density, specific heat, thermal conductivity). As well, typical compositions as determined by proximate and ultimate analysis were incorporated. Table 1 lists selected relevant particle properties. Three thousand particles were injected into the chamber in a uniform, randomly distributed manner throughout the porous fuel bed zone. Each particle was injected with zero initial velocity and an initial temperature of 320 K.

Table 1: Selected Properties of Discrete Straw Particles

Property	**Value**	**Units**
Diameter (d)	2.5	mm
Density (ρ)	410	kg/m^3
Specific heat (Cp)	1250	J/kg-K
Thermal conductivity (k)	0.05	W/m-K
Volatile component (by mass)	79.28	%
Fixed carbon component (by mass)	16.03	%
Ash component (by mass)	4.69	%
Moisture (by mass)	12	%
Carbon (by mass)	47.25	%
Hydrogen (by mass)	7.81	%
Oxygen (by mass)	44.94	%

In reality, the straw fuel bed is composed of straw particles stacked on top of each other. This stacking behaviour cannot be accurately modeled in Fluent; thus, an approach was

required to simulate a stationary bed. The solution was to use UDFs to keep the straw particles stationary in the fuel bed until the majority of their mass was released during evaporation, devolatization, and combustion. Two UDFs were written: one to set the drag coefficient on each particle to a very low value; and the second to impose a body force on the particle to counteract gravity. To avoid division-by-zero errors, the drag coefficient could not be set right to zero; thus, the particles did experience a small drag and would move a relatively short distance before the threshold mass was reached. Once this threshold mass was reached (4.5% of the initial mass), the particle was released to either fly away or fall out, since the particles were assumed to be no longer constrained within the straw fiber matrix.

4.8 Species transport and reaction model

The full "species transport" model was employed to simulate the transport and reaction of chemical species within the gasifier. Volumetric reactions were enabled, and the eddy-dissipation model was used to represent the interaction between turbulence and chemical reactions. Thus, neither reaction kinetics nor equilibrium chemistry was used to determine the chemical reactions; reaction rates were dependent strictly on turbulent mixing. Five chemical reactions were defined as follows:

Decomposition of volatiles:

$$CH_{3.06}O_{1.11}(g) \rightarrow 0.6CO + 0.254CO_2 + 0.146H_2 + 1.238CH_4 \quad (10)$$

Combustion of CO:

$$CO + 0.5O_2 \rightarrow CO_2 \quad (11)$$

Combustion of CH4:

$$CH_4 + 1.5O2 \rightarrow CO + 2H_2O(g) \quad (12)$$

Combustion of H2:

$$H_2 + 0.5O_2 \rightarrow H_2O(g) \quad (13)$$

Water-gas shift reaction:

$$CO + H_2O(g) \leftrightarrow CO_2 + H_2 \quad (14)$$

The volatiles "molecule", $CH_{3.06}O_{1.11}$, is meant to symbolize the variety of volatile compounds released via pyrolysis. The chemical subscripts for H and O elements within this molecule represent the ratio of H:C and O:C respectively, after subtracting the fraction of C that goes to fixed carbon (char). The heat of formation of this molecule, $H_{f,CH3.06O1.11}{}^{0}$, is determined by first taking its HHV to be:

$$HHV_{volatiles} = \frac{HHV_{fuel} - f_{char} HHV_{char}}{f_{volatiles}} \quad (15)$$

where f_{char} and $f_{volatiles}$ are the molar fractions of fixed carbon and volatiles, respectively. Then,

$$H_{f,CH3.06O1.11}{}^{0} = aH_{f,H2O(l)}{}^{0} + bH_{f,CO2} + HHV_{volatiles} \quad (16)$$

where a and b are the molar fractions of the combustion products, $H_2O(l)$ and CO_2.

4.9 Summary of cases studied

Overall, approximately 40 cases were studied during the development of this model. The majority of these cases were run to gain an understanding of how various parameters affected the solution. The 3D model was built according to the following procedure; test cases were run after each step.

1. Create the gasifier chamber geometry and computational grid using GAMBIT.
2. Set up the momentum and turbulence parameters and boundary conditions, and solve for a basic cold-flow case.
3. Incorporate the porous media zone.
4. Turn on energy and radiation equations, and incorporate the combustion of straw volatiles, injected into the chamber as a gas.
5. Inject combusting particles into the chamber.
6. Develop and incorporate UDFs that hold combusting particles stationary in the fuel bed zone until sufficient combustion has taken place.

The addition of combusting particles increased the complexity of the problem dramatically. As a result, convergence behaviour was greatly affected. In order to achieve realistic and converged solutions, the under-relaxation factors were greatly reduced. Typically, under-relaxation factors of 0.05-0.1 were necessary. The "Number of Continuous Phase Iterations per DPM Iteration" was also an important factor in achieving convergence; it was found that a value of at least 200 was required to maintain the stability of the solution. Convergence criteria based on the scaled sum of residuals over all nodes were taken as 10^{-4} for most of the equations, with the exception of continuity (10^{-3}), energy (10^{-5}) and P1 (10^{-6}). Typically, the number of iterations to convergence was on the order of 10 000 to 20 000.

4.10 Comparison to empirical data

Some attempt was made to compare the results of the 3D and equilibrium models to actual data collected from the Vidir biomass combustor at Arborg, MB. However, deficiencies in the control and instrumentation systems for this combustor undermined the usefulness of these comparisons. The following problems must be addressed before any meaningful comparison can be made:

1. Measurement of the actual airflow supplied to the primary chamber is incorrect. When compared against theoretical calculations, the measured flow rate of air into the chamber is much too low. This means that supplementary air must be entering the chamber from uninstrumented locations.

2. No means of measuring the composition of the syngas directly after the primary chamber exists. This would be necessary to verify the syngas compositions predicted by the numerical models.
3. The primary air flow rate is controlled not directly, but indirectly, by controlling the pressure drop through the fuel bed. The pressure drop through the bed is in turn controlled by adjusting the fuel feed rate, and thus, the height of the bed. This configuration thus demands that the mass flow rates of fuel and air into the primary chamber are not independent of each other, but are linked through the pressure drop. In other words, fuel feed rate and air flow rate cannot be controlled separately.

Each of these issues will be addressed more thoroughly in the Results section.

5.0 Results

5.1 Overview

Three final cases will be presented in this section, each with a different air flow rate. Case 1 corresponds to approximately 50% substoichiometric air, with an air-to-fuel ratio of 2.58. Case 1 was predominantly used during the development of the model. Cases 2 and 3 correspond respectively to half and double the air flow rate of Case 1; that is, approximately 75% substoichiometric air for Case 2 and 25% substoichiometric air for Case 3. All other problem parameters remained constant for these three cases. Table 2 provides a summary of the three cases studied.

Table 2: Summary of cases studied

Case	1	2	3
Run name	gasifier012508	gasifier012908	gasifier012908a
Run date	01/25/08	01/29/08	01/29/08
Fuel rate (kg/s)	0.062	0.062	0.062
Air flow rate (kg/s)	0.16	0.08	0.24
Air-to-fuel ratio (mass)	2.5806	1.2903	3.8710
% Substoichiometric air	50.563	75.281	25.844
Tout (K)	1439.3	1084.7	2152.8
Tmax (K)	1945.5	2008.0	2313.5
Pressure drop (Pa)	-1.8076	-0.2072	-3.6881
HHV (kJ/m3) at STP	1894.7	3902.3	210.89
LHV (kJ/m3) at STP	1700.4	3501.8	189.40

Results for the following output parameters will be examined in detail:

- Temperature
- Syngas composition
- Syngas heating values (HHV and LHV)
- Pressure drop across fuel bed
- Discrete phase model results

5.1 Temperature results

For each case, the peak and outlet temperatures produced by the 3D model were considered. These temperatures were compared with the temperatures predicted by the equilibrium model, as well as an overall heat balance. The heat balance was performed by calculating the overall heat of reaction as the difference between the enthalpies of the products and the enthalpies of the reactants, or:

$$\dot{Q}_{reaction} = \sum_{\text{products}} \dot{m}_i H^0_{f,i} - \sum_{\text{reactants}} \dot{m}_j H^0_{f,j} \tag{17}$$

The heat balance calculation was constrained by a mass balance on each element (C,H,O, and N) involved. Unburned char was considered in this calculation. However, the product

composition could not be matched exactly to that produced by the 3D model, due to the mass imbalance created by aborted particles. Typically, the difference for each component was less than 1%, with a few exceptions. The problem of aborted particles will be discussed in a later section. To allow for direct solution, a linear relationship between C_P and T was assumed for each of the component gases. This is in contrast to the piecewise-polynomial functions used in Fluent.

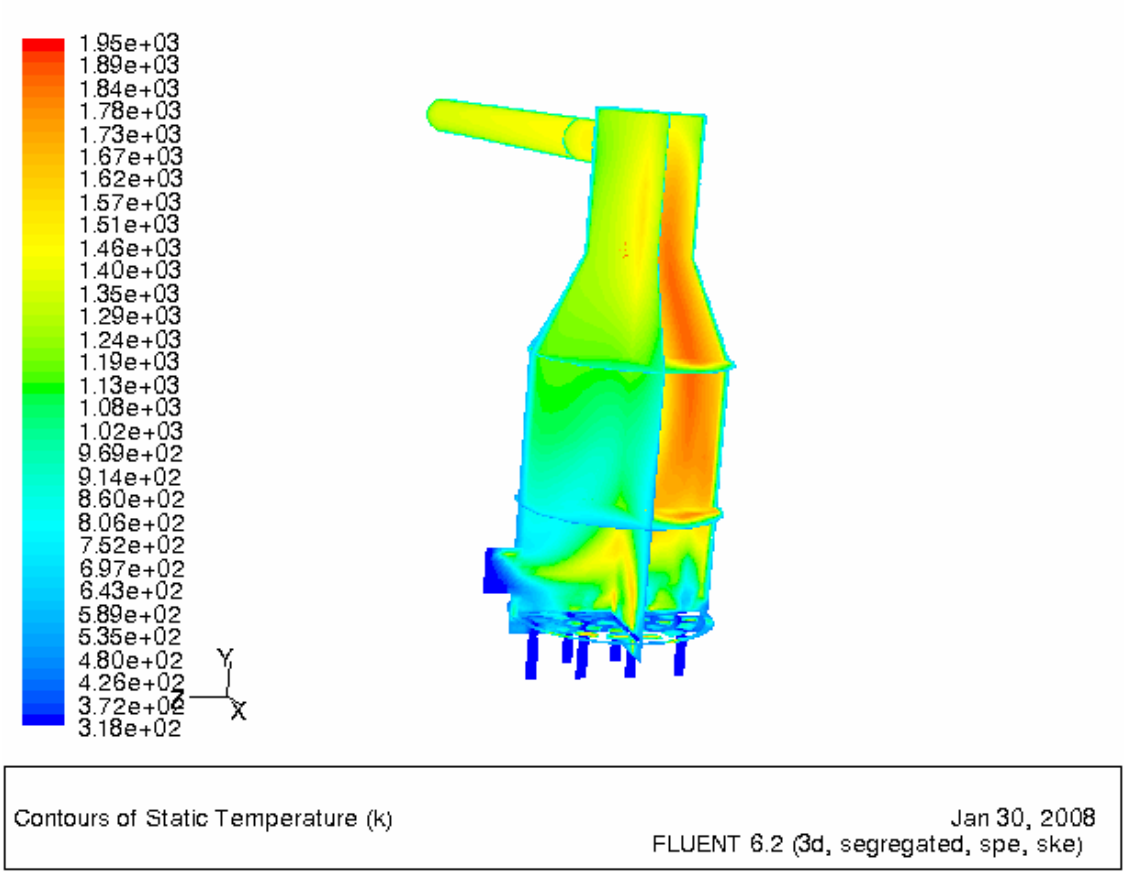

Figure 5: 3D temperature contours for Case 1, 50% Substoichiometric air

The 3D temperature contours for Case 1 are shown in Figure 5. A hot zone can be seen on the right side of the gasifier; this is due to the cold air coming from the side fuel port. Figure 6 shows the peak and outlet temperatures for all three cases. As expected, the outlet temperature shows an obvious decreasing trend as airflow decreases (or percentage below stoichiometric air increases) from 2150 K at 25% substoichiometric to 1440 K at 75% substoichiometric.

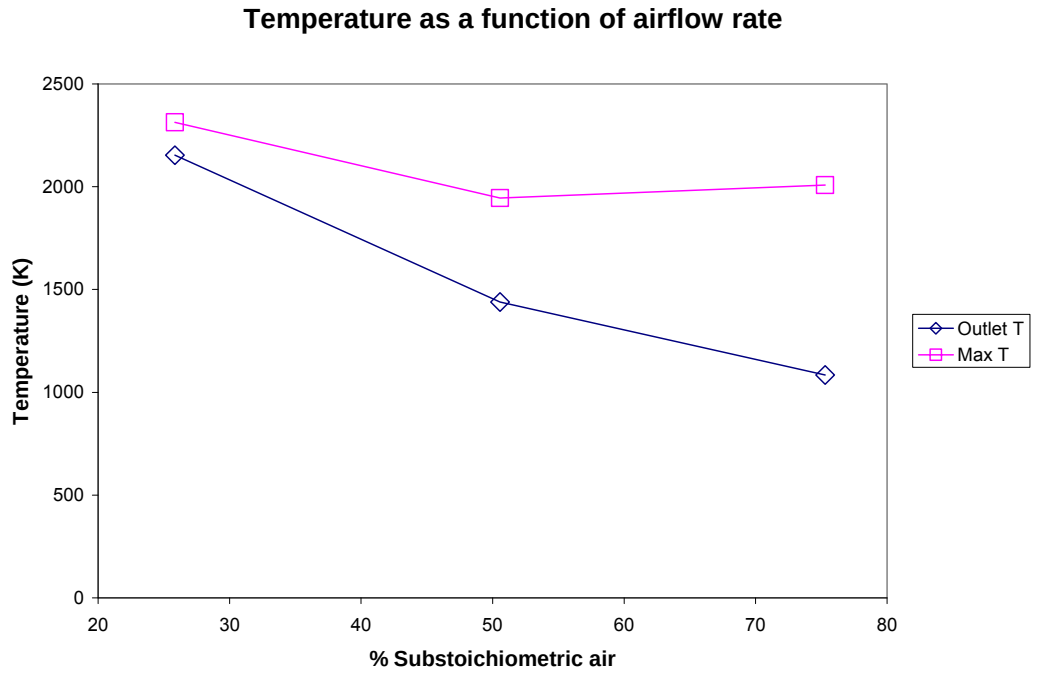

Figure 6: Temperatures results for the 3D model

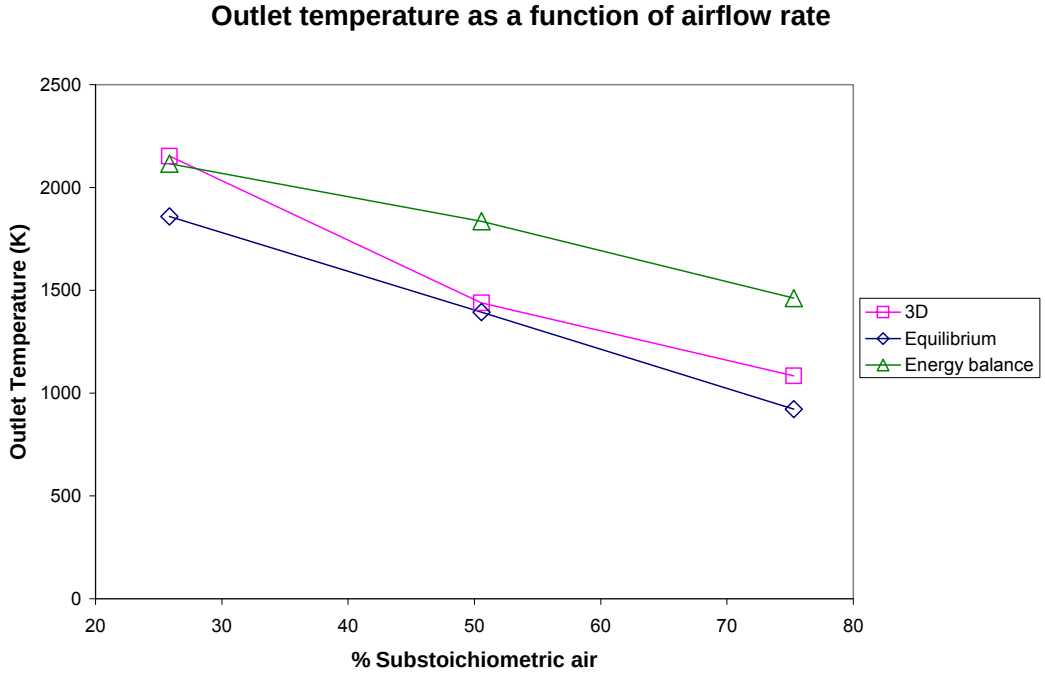

Figure 7: Comparison of temperature results

The outlet temperatures are compared to the temperatures predicted by the equilibrium model as well as the heat balance in Figure 7. In general, the equilibrium model predicts lower temperatures than the 3D model, while the heat balance predicts higher temperatures. The difference between the temperatures produced by the 3D and equilibrium models is caused mostly by differences in the predicted syngas composition (see next section). In comparison to the heat balance, however, the 3D model grossly underpredicts the outlet temperature for both the 50% and 75% cases (Cases 1 and 2). The differences in temperature for these two cases are 397 K and 377 K respectively, corresponding to differences of approximately 22% and 26%. The most probably cause of these differences lies in the assumption of linear C_P functions for the heat balance, as opposed to the piecewise-polynomial C_P functions used in Fluent.

5.2 Syngas composition results

Three-dimensional composition results for Case 1 are found in Figures 8, 9, 10, and 11. Composition of oxygen, carbon monoxide, carbon dioxide, and water vapour are shown. A full collection of 3D results is found in the appendix. Notice that the oxygen is depleted fairly quickly at the bottom of the chamber.

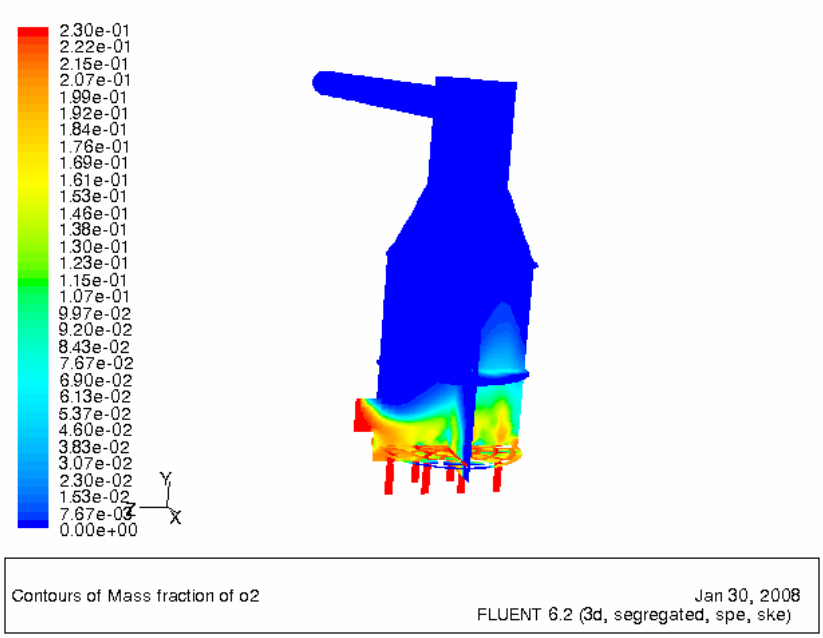

Figure 8: Mass composition of O_2 for Case 1, 50% substoichiometric air

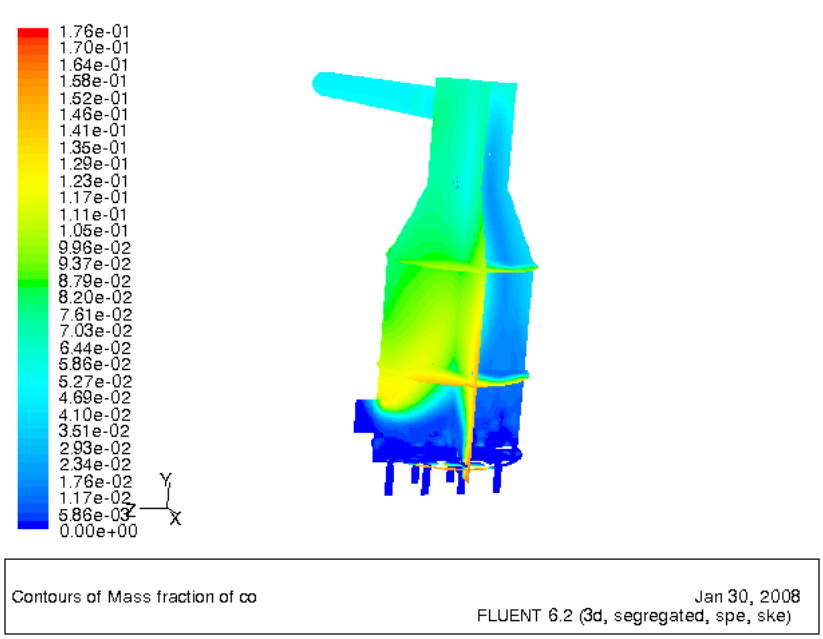

Figure 9: Mass composition of CO for Case 1, 50% substoichiometric air

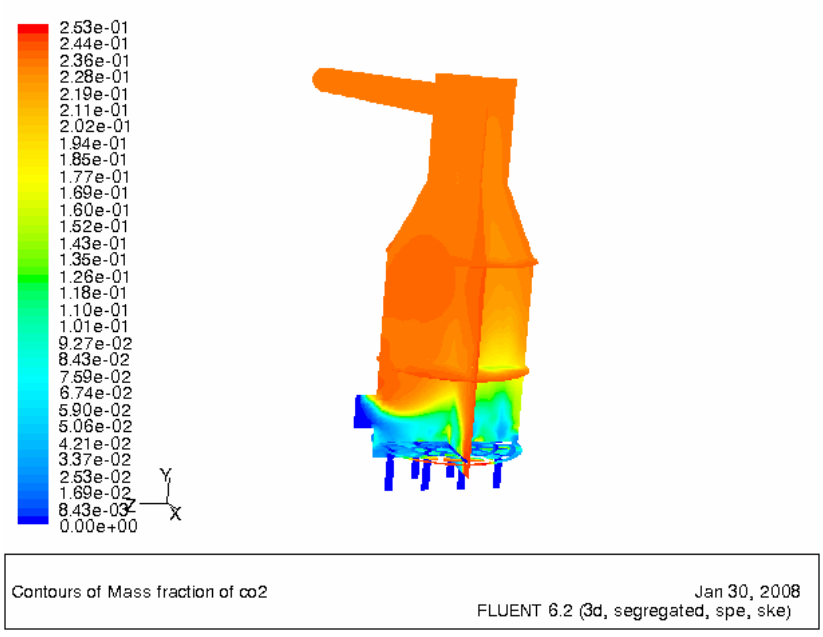

Figure 10: Mass composition of CO_2 for Case 1, 50% substoichiometric air

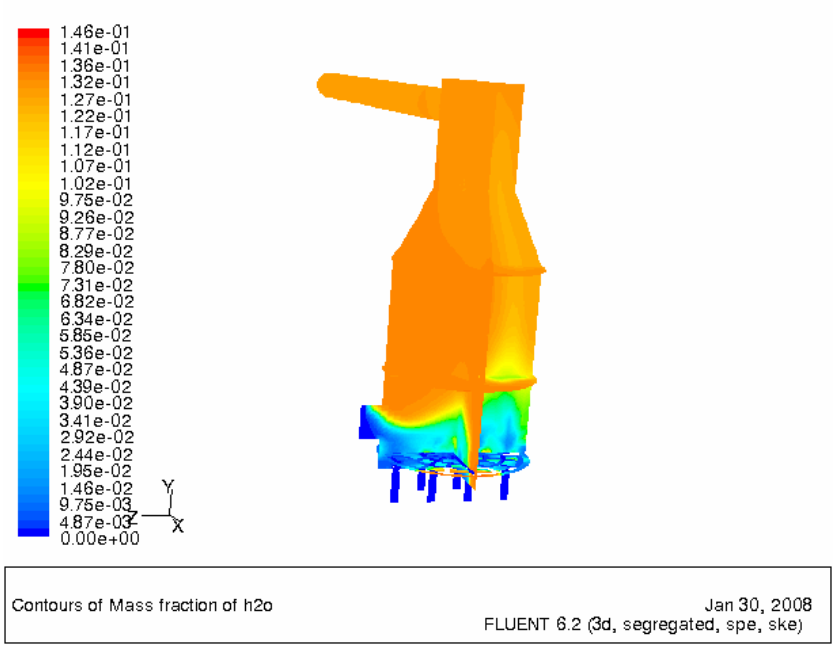

Figure 11: Mass composition of $H_2O(g)$ for Case 1, 50% substoichiometric air

The syngas composition present at the outlet of the primary gasification chamber is of particular interest. Figures 12a and 12b display the syngas composition as predicted by the 3D model. As the supply of air is increased, it is evident that the volume fractions (and thus, molar fractions) of H_2, CO, and CH_4 decrease, while the volume fractions of $H_2O(g)$, N_2, and CO_2 increase. Similar trends are noticed in the mass fractions, with the exception of $H_2O(g)$ and CO_2. It is surprising that the fraction of CO2 only changes slightly between cases; however, the mass flow of CO_2 at the outlet does increase with increasing airflow, since the total outlet mass flow is increasing.

Figures 13a and 13b show the syngas composition as predicted by the equilibrium model. Similar trends can be seen for most of the component gases, with the exception of CO_2. As well, the fraction of water vapour increases much more dramatically in the equilibrium model, as opposed to the 3D model. The differences between equilibrium model results and 3D results are shown in Figures 14a and 14b. In comparison with the equilibrium model, the 3D model overpredicts the fractions of CO_2, $H_2O(g)$, and N_2, while the fractions of H_2, CO, and CH_4 are underpredicted. The largest differences between the two models occur for the components of CO and $H_2O(g)$.

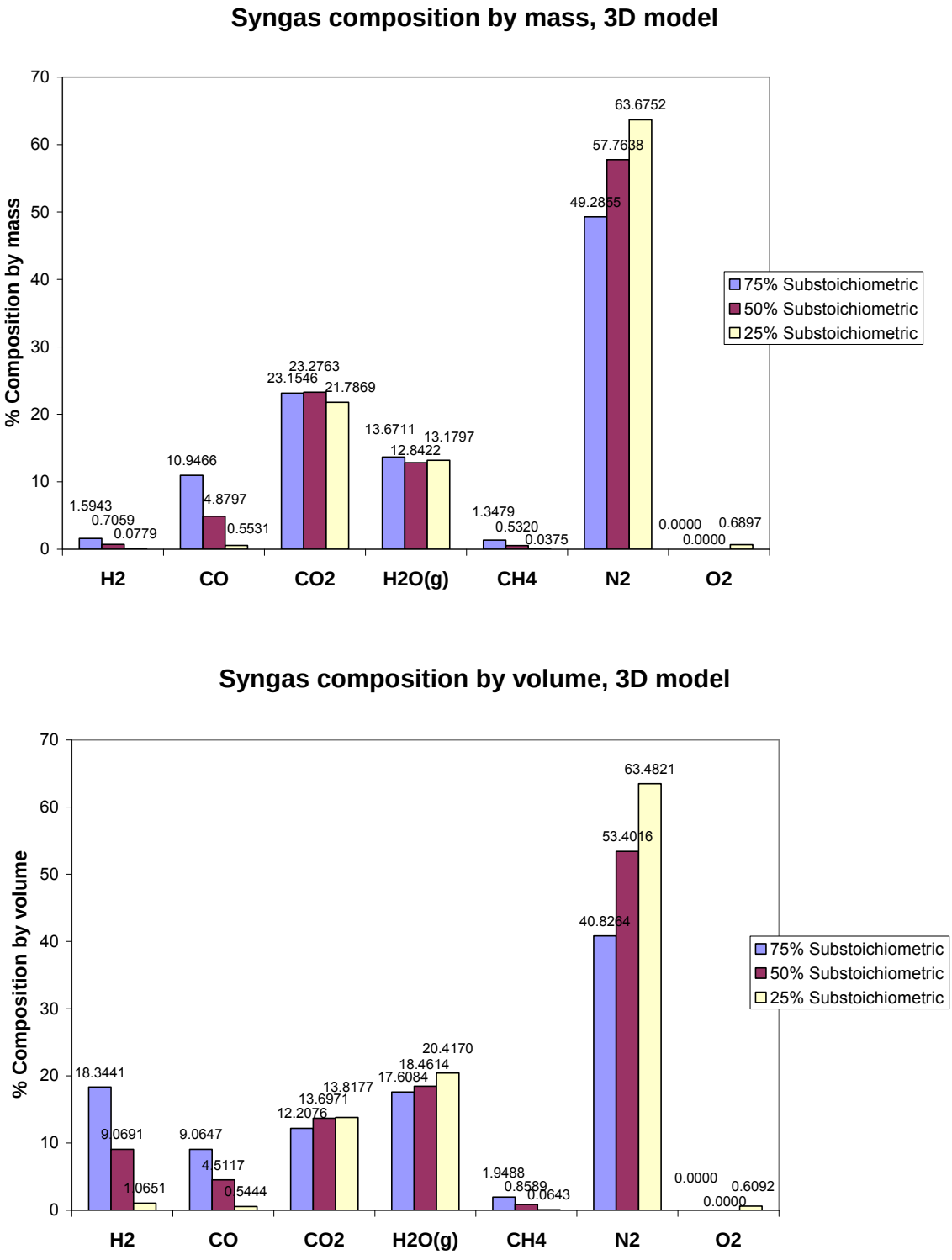

Figures 12a and 12b: Syngas composition as predicted by 3D model

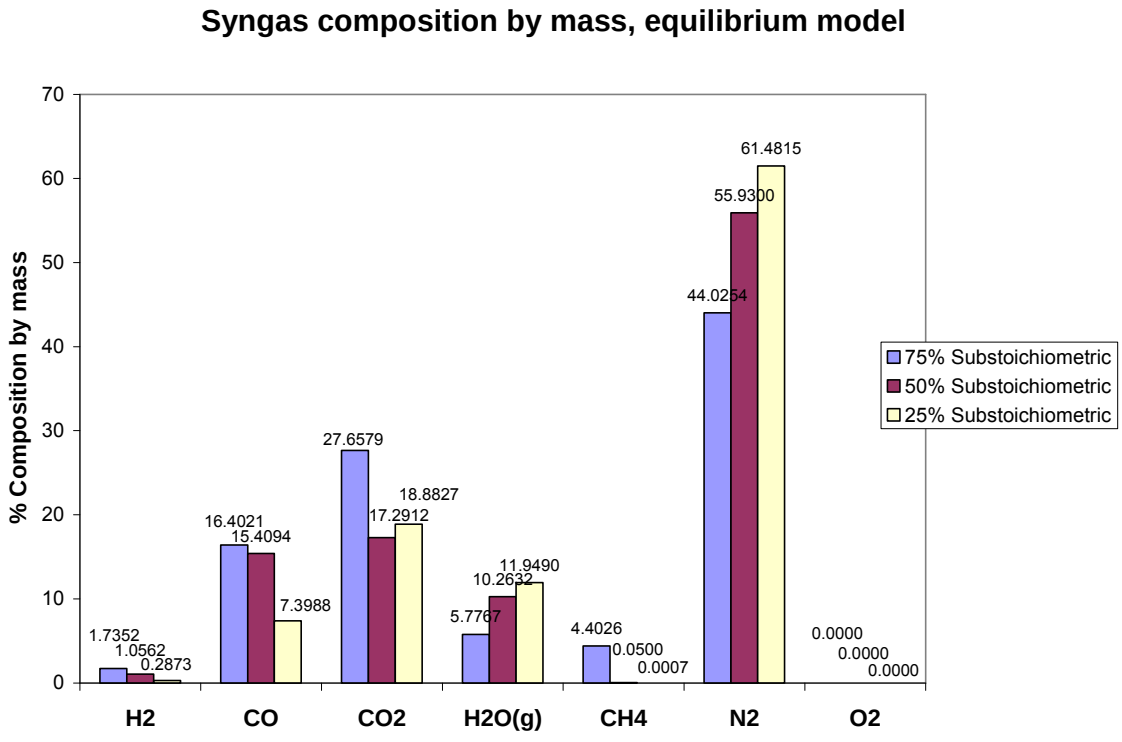

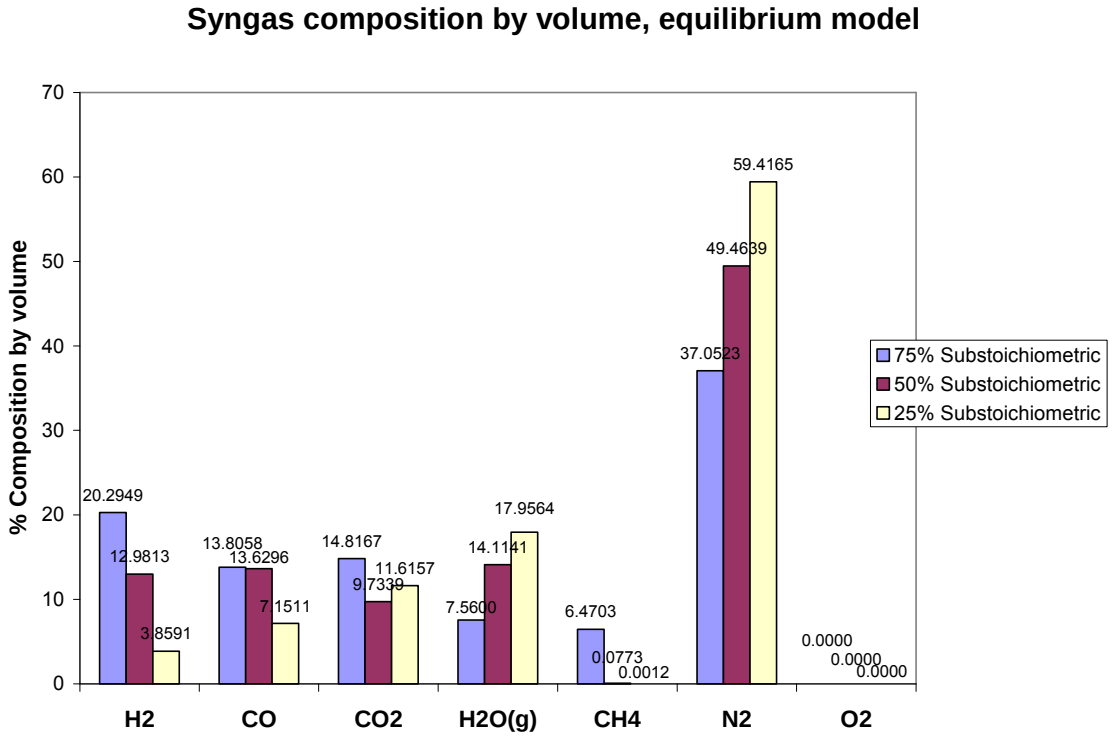

Figures 13a and 13b: Syngas composition as predicted by equilibrium model

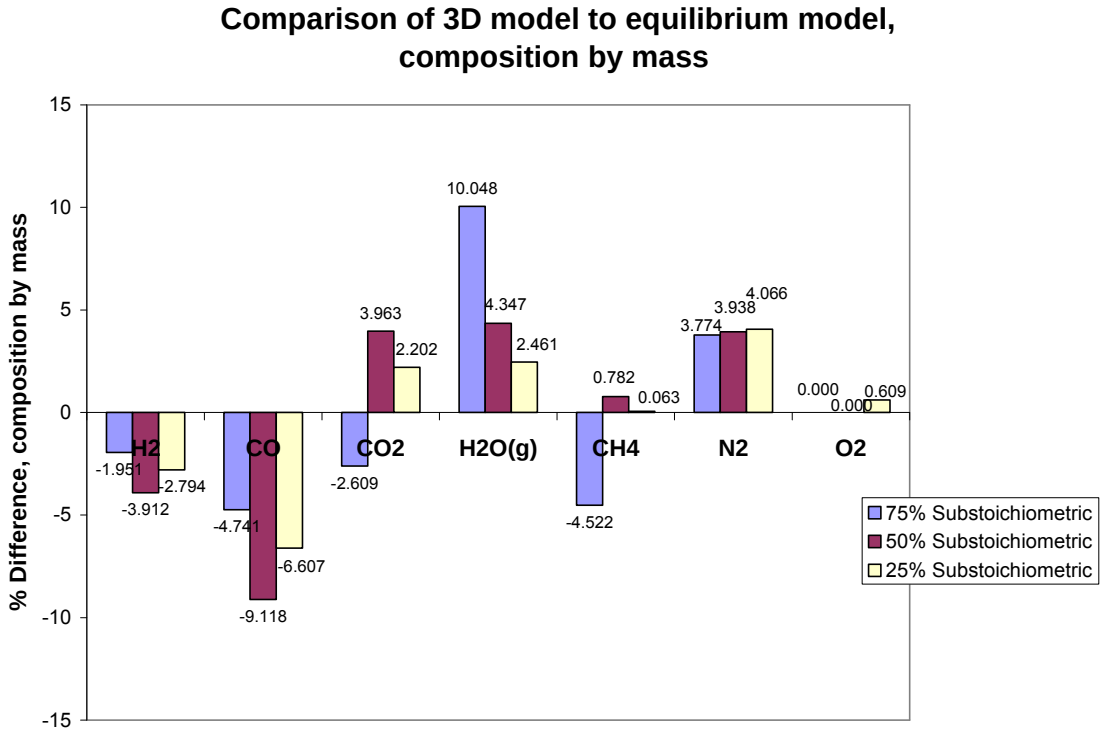

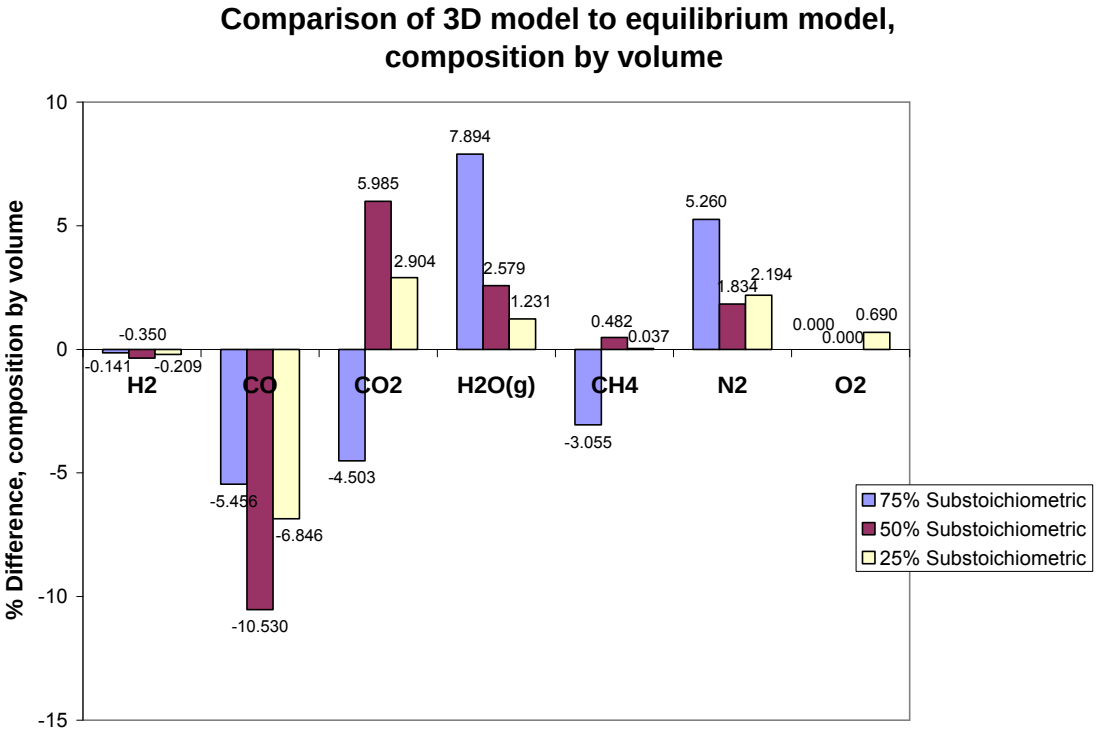

Figures 14a and 14b: Syngas composition, percent difference between 3D model and equilibrium model

Table 3: Syngas composition, 3D model

Case	1	2	3
% Substoichiometric	**50.5630**	**75.2815**	**25.8445**
% mass H2	0.7059	1.5943	0.0779
% mass CO	4.8797	10.9466	0.5531
% mass CO2	23.2763	23.1546	21.7869
% mass H2O(g)	12.8422	13.6711	13.1797
% mass CH4	0.5320	1.3479	0.0375
% mass N2	57.7638	49.2855	63.6752
% mass O2	0.0000	0.0000	0.6897
% mass total	100.0000	100.0000	99.9999
% vol. H2	9.0691	18.3441	1.0651
% vol. CO	4.5117	9.0647	0.5444
% vol. CO2	13.6971	12.2076	13.8177
% vol. H2O(g)	18.4614	17.6084	20.4170
% vol. CH4	0.8589	1.9488	0.0643
% vol. N2	53.4016	40.8264	63.4821
% vol. O2	0.0000	0.0000	0.6092
% volume total	99.9997	100.0000	99.9999
% char conversion	32.14	5.77	38.15

Table 4: Syngas composition, equilibrium model

Case	1	2	3
% Substoichiometric	**50.5630**	**75.2815**	**25.8445**
% mass H2	1.0562	1.7352	0.2873
% mass CO	15.4094	16.4021	7.3988
% mass CO2	17.2912	27.6579	18.8827
% mass H2O(g)	10.2632	5.7767	11.9490
% mass CH4	0.0500	4.4026	0.0007
% mass N2	55.9300	44.0254	61.4815
% mass O2	0.0000	0.0000	0.0000
% mass total	100.0000	100.0000	100.0000
% vol. H2	12.9813	20.2949	3.8591
% vol. CO	13.6296	13.8058	7.1511
% vol. CO2	9.7339	14.8167	11.6157
% vol. H2O(g)	14.1141	7.5600	17.9564
% vol. CH4	0.0773	6.4703	0.0012
% vol. N2	49.4639	37.0523	59.4165
% vol. O2	0.0000	0.0000	0.0000
% volume total	100.0000	100.0000	100.0000
% char conversion	100.00	100.00	100.00

Tables 3 and 4 summarize the syngas composition results. The fraction of fixed carbon present in the fuel that was converted through combustion is also shown in Table 3. In general, under 40% of the char was converted; in Case 2, char conversion is as low as

5.77%. These values may not reflect realistic results, and are probably due to inaccurate modeling of the straw particle motion through the gasifier. This will be discussed in further detail later in the report. The equilibrium model assumes 100% char conversion.

5.3 Syngas heating value

The heating value of a fuel is the amount of energy released when that fuel is combusted. Higher heating value (HHV) is the heat of combustion when the product water is in liquid state; lower heating value (LHV) is the heat of combustion when the product water is in vapour state. The HHV and LHV predicted by the 3D model are shown in Figure 15 and compared to the equilibrium model predictions.

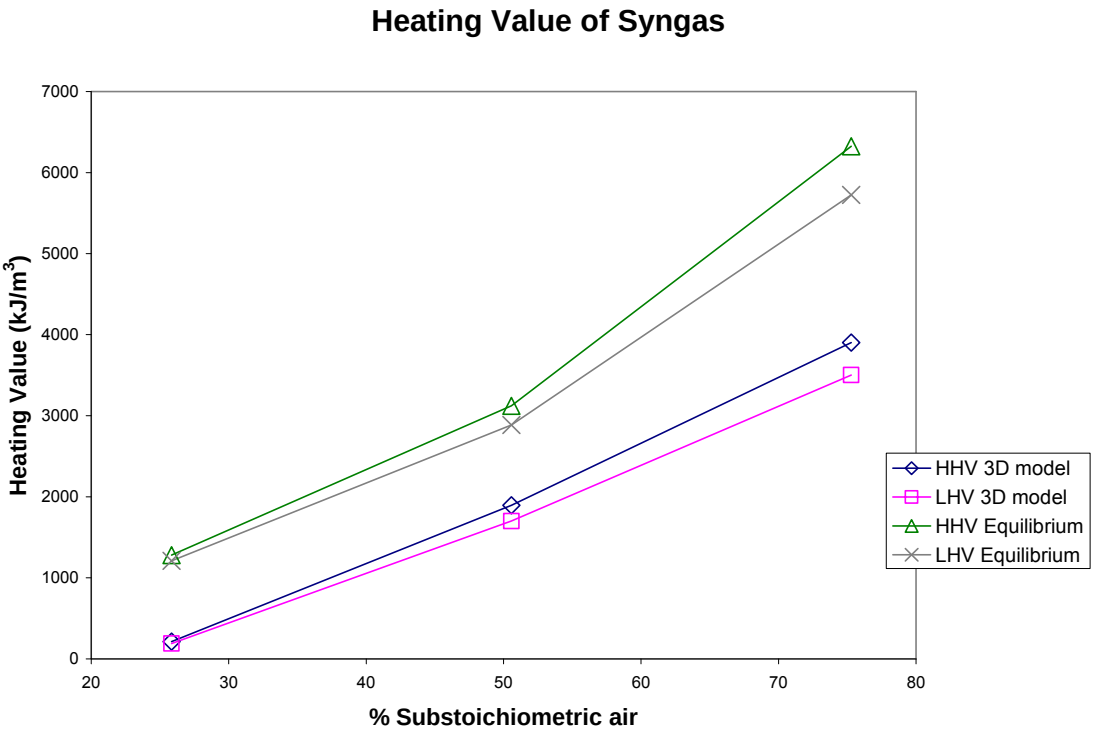

Figure 15: HHV and LHV of the syngas; 3D model compared to equilibrium model

There is a large difference between the heating values predicted by the two models – over 1000 kJ/m^3 in all three cases. The major reason for this difference is the presence of unconverted char in the 3D model. Incomplete char conversion means more CO_2 and less CO in the product gas, which decreases the heating value considerably. In the case of 75 % substoichiometric air, in which only 5.77% of the char is combusted, the difference is heating values is over 2400 kJ/m^3. The higher concentration of CO_2 produced also creates higher outlet temperatures, since the formation of CO_2 releases much more heat than the formation of CO.

5.4 Pressure drop across the fuel bed

The porous fuel bed present inside the gasifier chamber adds another degree of complexity to the simulation. The porous media zone in the bottom half of the chamber affects momentum, radiation, and energy equations directly; therefore, indirectly the whole model is affected. The pressure drop across the fuel bed was measured; more specifically, the difference in the cross-sectional average pressure between the top of the fuel bed and the bottom of the chamber was calculated for each case. The results are shown in Figure 16. As expected, pressure drop increases with air flow; however, the pressure drop is never more than a few pascals. Note that Figure 16 is plotted as a function of the mass flow rate of air, rather than the percentage below substoichiometric air.

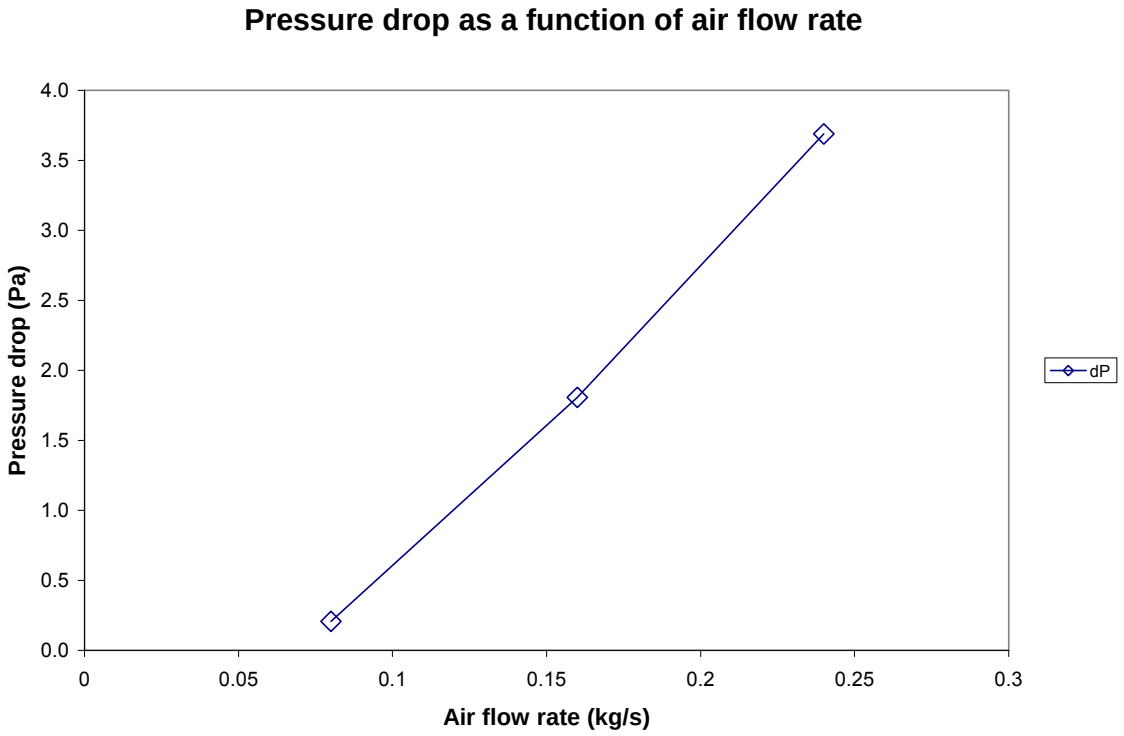

Figure 16: Pressure drop across the porous fuel bed

5.5 Discrete phase results

A summary of the results for the discrete phase model is shown in Table 5; the trajectories of a sample of 100 particle streams are shown in Figure 17. In general, the moisture content of the fuel particles was almost completely evaporated; likewise, nearly complete pyrolysis was achieved. Case 2 was the exception, with over 5% of the total volatile content remaining unconverted. As mentioned earlier, the char conversion for Case 2 was exceptionally low.

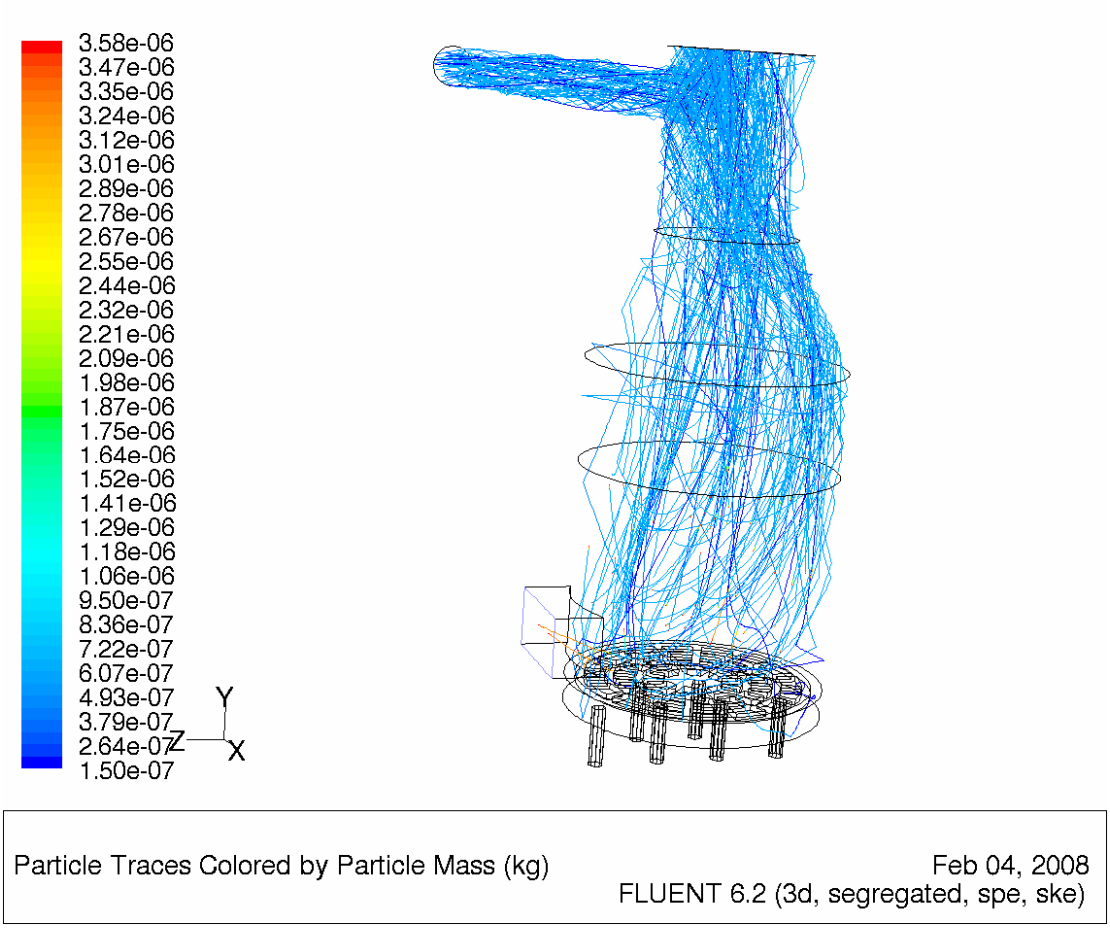

Figure 17: Discrete phase particle trajectories for Case 1, 50% substoichiometric air

Apart from Case 2, the number of aborted particles was kept reasonably low (under 25%). In the Case 2 simulation however, 82.4% of all particle streams were aborted before their trajectories were complete. Aborted particles generally occur due to the accumulation round-off errors during the trajectory calculation. It was noticed that aborted particles only occurred when the stationary particle UDFs were employed. This problem will be the object of future consideration, with the hope of being able to significantly reduce the number of aborted particles. One factor to consider is the size, and geometry of the particles. Perhaps by adjusting these parameters to best reflect the aerodynamic characteristics of the particles rather than strictly the physical characteristics, a better representation of particle motion can be achieved. It should be noticed that in Figure 17, nearly all of the particles fly up and out the exit of the chamber; in reality, more ash particles should fall to the bottom to be removed by the ash auger.

Table 5: Discrete phase summary

Case	1	2	3
% Substoichiometric	**50.5630**	**75.2815**	**25.8445**
Aborted particles	691	2472	437
Incomplete particles	64	3	5
Escaped particles	2245	510	2558
Change in mass (kg/s)	-0.05317	-0.04871	-0.05368
Change in enthalpy (kW)	456.28	436.05	465.56
% Moisture evaporated	99.93	99.90	99.93
% Volatiles converted	99.49	94.69	99.45
% Char converted	32.14	5.77	38.15

5.6 Comparison with experimental data

Some experimental data was provided by Vidir, based on a run of the Arborg BEST on July 18, 2007. Straw was used as fuel. Data was recorded during the "start-up" and "running mode" phases of the run, over a period of 84 minutes. From this data, the average conditions during "running mode" were considered; the relevant parameters are presented in Table 6.

Table 6: Average conditions for straw run of the Arborg BEST

Parameter	Value	Unit
Primary temperature	916.9	K
Primary mid-chamber temperature	796.1	K
System gauge pressure	-0.174	kPa
Avg. fuel mass flow rate ("Current")	0.0616	kg/s
Avg. fuel mass flow rate ("Hourly")	0.0735	kg/s
Primary air volume flow rate	0.00275	m3/s
Primary air mass flow rate	0.00301	kg/s
Primary air inlet temperature	319.8	K

From this data, certain values could be used as valid parameters for the numerical simulations. Specifically, the average current mass flow rate of straw fuel was used as the total flow rate of straw particles in all test cases (0.062 kg/s). As well, an inlet temperature of 320 K was used in all simulations.

However, the flow rate of air to the primary chamber could not be used, as it is unrealistic. This value, 0.00301 kg/s of air, corresponds to a substoichiometric value of 99.07%; in other words, this amount of air would only supply 0.93% of the fuel's oxygen demand. With this little oxygen supplied to the system, there would be no possibility of sustaining any sort of reaction at all. Therefore, one of two conclusions must be made: either the calibration of the flow meter is incorrect; or a substantial amount of air is entering the primary chamber at a different location. There are three such locations at which unknown quantities of air may be entering the chamber:

1. Through the fuel port.

2. Through the ash auger
3. Through leaks in the walls of the chamber.

It is most likely that air enters through the fuel port. This port is open to fresh air from outside the system when the fuel ram is retracted. Since the fuel port is approximately midway to the top of the fuel bed, air entering there would encounter much less resistance to flow from the packed straw. As well, since the clearance between the ram and the fuel port is fairly small, it is very possibly that the ram is actually acting as a pump to push fresh air into the system. Whatever the case may be, it is almost certain that a large volume of air is entering the primary chamber via this route. Taking this into account, in the development of the 3D model, air was introduced to the gasification chamber through both the primary air inlets as well as the fuel port.

An attempt was made to predict the gauge pressure of the system by calculating within the 3D model the pressure drop from the bottom of the chamber to the top of the fuel bed. The resulting calculations showed a pressure drop of less than 5 Pa for all runs; however, the measured gauge pressure of the system is -174 Pa. This is because the 3D model cannot predict accurately the pressure drop of the air inlet system without incorporating the geometry of the inlet system in great detail; this would add unmerited complexity to the system. As well, the exact location of the pressure flow meter was not considered in the calculation. For validation purposes, a better approach would be to measure the pressure at two or three locations (ie. beneath the grate, above the fuel bed, and at the top of the chamber) and compare the relative pressures to those given by the 3D simulations.

In general, the lack of knowledge of the exact locations of the instrumentation hindered useful comparison between the experimental data and the 3D simulation. To remedy this, a detailed diagram of the location of all instruments should be prepared.

A significant problem emerges when considering the optimization of the Arborg BEST unit. The problem is that, due to the current means of controlling the unit, the fuel feed rate and the air flow rate cannot be independently varied. Currently, the flow rate of gas through the whole system is driven by a suction fan near the exit. This fan operates at a constant speed, and thus, creates a specified vacuum pressure that cannot be varied. To control the air flow into the primary chamber then, the flow resistance created by the biomass fuel bed is taken advantage of. To increase the flow of air, the fuel feed rate is decreased or stopped, decreasing the height of the fuel bed, and thus, the resistance to air flow through the bed. To decrease the flow of air into the chamber, the fuel rate is increased. The pressure inside the primary chamber is measured, and this value is used to determine whether to increase or decrease the fuel feed rate. The problem with this control system is that the air-to-fuel ratio is fixed, and cannot be varied. Since this air-to-fuel ratio is instrumental in determining the effectiveness of the gasification process, any attempt to improve the performance by controlling the primary to secondary air ratio is difficult. This is analogous to an internal combustion engine with a stuck carburetor. This also means that the air-to-fuel ratio cannot be varied to accommodate the type of fuel used, such as straw, wood chips, reed grass, or cattails. To add further a limitation, the

rotating grate within the chamber becomes overloaded at a certain bed height. When this happens, the feed rate of fuel must be stopped until the grate can rotate again.

6.0 Conclusion

Powerful computational fluid dynamics (CFD) software, such as Fluent, have become important tools in both the academic and industrial realms. By developing accurate, three-dimensional models of engineering systems, many "computer experiments" can be performed at a fraction of the cost of an actual experiment. Though numerical simulations cannot replace real-life testing, they can be used to predict trends and troubleshoot problems, allowing physical experimentation to be used more effectively.

The goal of this research project was to develop a 3D steady state model of a primary gasification chamber using a porous bed approach. This model will be incorporated into a larger project that aims at modeling the entire Vidir BEST two-stage combustor system. During the course of this research project, realistic geometry, flow conditions, and fuel properties were incorporated into a 3D numerical model using Fluent CFD software. A porous media zone, the behaviour of a discrete particle phase, and multi-step chemical reactions increased the complexity of the model. Additionally, a zero-dimensional, steady state spreadsheet model based on equilibrium chemical equations was produced, and the results were compared to the 3D model. Though each model was developed under a different set of initial assumptions, the comparison still proves useful in the absence of well-defined experimental data.

By performing simulations with approximately 25%, 50%, and 75% substoichiometric air, it was shown that the 3D model performed fairly well, and exhibited the expected trends for temperature, syngas composition, heating value of the syngas, and pressure drop. These trends were confirmed by results from the equilibrium spreadsheet model. Differences between the two sets of results can be explained satisfactorily by considering the set of assumptions for each model. Table 7 shows the relevant differences in assumptions.

Table 7: Differences in assumptions between 3D model and equilibrium model

3D model	**Equilibrium**
Non-equilibrium conditions	Equilibrium conditions
Possible incomplete char combustion	Complete char combustion
Piecewise-polynomial Cp's	Cp formula based on T_{in}, T_{out}, and T_{avg}
Heating of fuel particles and ash considered	Only heating of gases considered

Experimental data from the Arborg BEST was analyzed for comparison to the 3D model. However, flaws in the data prevented any useful comparison; the most significant of these flaws was the obvious error in the flow rate of air into the primary chamber. The measured rate of air would supply less than 1% of the total oxygen demand of the biomass fuel. It is most likely that a significant amount of supplementary air is supplied to the primary chamber through the fuel port.

7.0 Recommendations

Based on the results, discussion, and conclusions found in this report, the following actions are recommended:

1. It is recommended to incorporate the 3D porous bed model generated in this project into the 3D model of the full BEST system. While doing this, one must consider how to improve on some of the deficiencies encountered in this model. Specifically, the motion of straw particles through the primary chamber should be thoroughly investigated, along with the related issues of aborted particles and unburned char.
2. It is recommended that more instrumentation be installed on the Arborg BEST unit. Specifically, the following instrumentation should be installed:
    a. A method of measuring the air entering the primary chamber through the fuel port should be devised. As well, enough instrumentation must be installed to determine whether air is introduced to the system at other locations – possibly the ash auger, or leaks in the gasifier walls.
    b. The calibration of the flow meter on the primary air inlet should be checked.
    c. A method of sampling and analyzing the syngas prior to secondary combustion should be developed. The composition of the gas as it exits the primary chamber is necessary for proper comparison with the 3D model.
    d. Multiple pressure gauges should be installed to allow for the relative pressures to be recorded and compared.
    e. Multiple temperature sensors should be installed to give an accurate representation of the temperature distribution throughout the chamber. These sensors should be placed at varying vertical and horizontal heights.
    f. The moisture content of the fuel should be measured and recorded just prior to use in the BEST.
    g. The amount of ash produced during each run should be recorded to give a proper mass balance.
3. The system of controlling the air flow to the primary chamber by varying the height of the fuel bed is severely flawed and must be changed. Rather than relying on suction to pull an unknown amount of air from unknown locations into the primary chamber, air should be deliberately pumped in. In this way, the exact amount of air entering the system is known, and can be varied independently of the fuel rate.

8.0 References

[1] A. V. da Rosa, Fundamentals of Renewable Energy Processes, Elsevier Inc., San Diego, CA, 2005.

[2a] P. McKendry, 2002. Energy production from biomass (part 1): overview of biomass. Bioresource Technology. 83, 37-46.

[2b] P. McKendry, 2002. Energy production from biomass (part 2): conversion technologies. Bioresource Technology. 83, 37-46.

[2c] P. McKendry, 2002. Energy production from biomass (part 1): gasification technologies. Bioresource Technology. 83, 37-46.

[3] T. Rampling, 1993. Fundamental research on the thermal treatment of wastes and biomass: literature review of part research on thermal treatment of biomass and waste. ETSU B/T1/00208/Rep/1.

[4] T. Rampling and P. Gill, 1993. Fundamental research on the thermal treatment of wastes and biomass: thermal treatment characteristics of biomass. ETSU B/T1/00208/Rep/1.

[5] M. Ruggiero and G. Manfrida, 1999. An equilibrium model for biomass gasification processes. Renewable Energy 16. 1106-1109.

[6] Z. A. Zainal et. al., 2001. Prediction of performance of a downdraft gasifier using equilibrium modeling for different biomass materials. Energy Conversion and Management. 42, 1499-1515.

[7] P. Matthieu and R. Dubuisson, 2002. Performance analysis of a biomass gasifier. Energy Conversion and Management. 43, 1291-1299.

[8] Zhou et al., 2005. Numerical modeling of straw combustion in a fixed bed. Fuel. 84, 389-403.

[9] Powerpoint Presentation – Vidir GDS. [Online]. Retrieved Feb. 1, 2008. Available at: www.vidir.biz/vidirbiomass/vidirbiomass.ppt.htm.

[10] Fluent 6.1.22. Copyright 2003, Fluent Inc.

[11] GAMBIT 2.2.30. Copyright 1988-2008 Fluent Inc.

[12] Fluent 6.2 User's Guide. Copyright 2005, Fluent, Inc.

[13] Fluent 6.3 UDF Manual. Copyright 2006, Fluent, Inc.

[14] F. P. Incropera and D. P. DeWitt, Fundamentals of Heat and Mass Transfer, 5th ed., John Wiley and Sons, New York, 2002.

[15] Y. A. Cengel and M. A. Boles, Thermodynamics: An Engineering Approach. 4th ed., McGraw-Hill, 2002.

Appendix A: Summary of Results

Summary of runs

Case	1	2	3
Run name	gasifier012508	gasifier012908	gasifier012908a
Run date	01/25/08	01/29/08	01/29/08
Fuel rate (kg/s)	0.062	0.062	0.062
Air flow rate (kg/s)	0.16	0.08	0.24
Air to fuel ratio (mass)	2.5806	1.2903	3.8710
% Substoich	50.563	75.281	25.844
Tout (K)	1439.3	1084.7	2152.8
Tmax (K)	1945.5	2008.0	2313.5
Pressure drop (Pa)	-1.8076	-0.2072	-3.6881
HHV (kJ/kmol)	46339	95441	5158.0
HHV(kJ/kg)	13792	28008	1601.0
HHV (kJ/m3) at STP	1894.7	3902.3	210.89
LHV (kJ/m3) at STP	1700.4	3501.8	189.40

Summary of Composition

3D MODEL			
Run number	1	2	3
% Substoich	**50.5630**	**75.2815**	**25.8445**
% mass H2	0.7059	1.5943	0.0779
% mass CO	4.8797	10.9466	0.5531
% mass CO2	23.2763	23.1546	21.7869
% mass H2O(g)	12.8422	13.6711	13.1797
% mass CH4	0.5320	1.3479	0.0375
% mass N2	57.7638	49.2855	63.6752
% mass O2	0.0000	0.0000	0.6897
% char conversion	32.1400	5.7700	38.1500
% vol. H2	9.0691	18.3441	1.0651
% vol. CO	4.5117	9.0647	0.5444
% vol. CO2	13.6971	12.2076	13.8177
% vol. H2O(g)	18.4614	17.6084	20.4170
% vol. CH4	0.8589	1.9488	0.0643
% vol. N2	53.4016	40.8264	63.4821
% vol. O2	0.0000	0.0000	0.6092
% mass total	100.0000	100.0000	99.9999
% volume total	99.9997	100.0000	99.9999

EQUILIBRIUM MODEL			
Run number	1	2	3
% Substoich	50.5630	75.2815	25.8445
% mass H2	1.0562	1.7352	0.2873

% mass CO	15.4094	16.4021	7.3988
% mass CO2	17.2912	27.6579	18.8827
% mass H2O(g)	10.2632	5.7767	11.9490
% mass CH4	0.0500	4.4026	0.0007
% mass N2	55.9300	44.0254	61.4815
% mass O2	0.0000	0.0000	0.0000
% char conversion	N/A	N/A	N/A
% vol. H2	12.9813	20.2949	3.8591
% vol. CO	13.6296	13.8058	7.1511
% vol. CO2	9.7339	14.8167	11.6157
% vol. H2O(g)	14.1141	7.5600	17.9564
% vol. CH4	0.0773	6.4703	0.0012
% vol. N2	49.4639	37.0523	59.4165
% vol. O2	0.0000	0.0000	0.0000
% mass total	100.0000	100.0000	100.0000
% volume total	100.0000	100.0000	100.0000

% DIFFERENCE

Run number	1	2	3
% Substoich	50.563	75.281	25.844
% mass H2	-0.350	-0.141	-0.209
% mass CO	-10.530	-5.456	-6.846
% mass CO2	5.985	-4.503	2.904
% mass H2O(g)	2.579	7.894	1.231
% mass CH4	0.482	-3.055	0.037
% mass N2	1.834	5.260	2.194
% mass O2	0.000	0.000	0.690
% char conversion	N/A	N/A	N/A
% vol. H2	-3.912	-1.951	-2.794
% vol. CO	-9.118	-4.741	-6.607
% vol. CO2	3.963	-2.609	2.202
% vol. H2O(g)	4.347	10.048	2.461
% vol. CH4	0.782	-4.522	0.063
% vol. N2	3.938	3.774	4.066
% vol. O2	0.000	0.000	0.609

DPM Summary

Run number	1	2	3
% Substoich	50.5630	75.2815	25.8445
Aborted particles	691	2472	437
Incomplete particles	64	3	5
Escaped particles	2245	510	2558
Change in mass (kg/s)	-0.05317	-0.04871	-0.05368
Change in enthalpy (kW)	456.28	436.05	465.56
% Moisture evaporated	99.93	99.90	99.93
% Volatiles converted	99.49	94.69	99.45
% Char converted	32.14	5.77	38.15

Temperature Comparison

Run number	Model	1	2	3
Tout (K)	3D	1439.3	1084.7	2152.8
Tout (K)	EQ	1394.0	922.0	1859.0
Tout (K)	Stoich	1835.9	1462.0	2115.9
Tmax (K)	3D	1945.5	2008.0	2313.5

Appendix B: Equilibrium Model Spreadsheet

Sheet 1: Model

Gasifier Model - version 1

Assumptions:

1. Assume that the syngas composition is known
2. Assume that the gasifier chamber is at constant temperature, and this temperature is known.
3. Assume fuel can be written as CxHyOz
4. Write overall reaction, instead of each individual reaction
5. Ignore reaction kinetics, Gibbs energy. Assume reaction is governed strictly by the balanced equation.
6. Assume dry air is used.

Overall Reaction:

CHaOb + w*H2O + m*(O2+3.76N2) => x1*H2 + x2*CO + x3*CO2 + x4*H2O + x5*CH4 + 3.76m*N2

where:

- a = y_H/y_C
- b = y_O/y_C
- w = MM_{fuel}*MC/(MM_{H2O}*(1-MC))
- m = moles air per mole fuel

Fuel Composition

	% mass	mass fraction	Molar Mass	mfi/Mi	mole fraction (yi)	dry %mass
C	40.20890625	0.402089063	12.0107	0.033477571	0.2589769	45.033975
H	6.646170536	0.066461705	1.0079	0.065940773	0.510106812	7.443711
O	38.2431375	0.382431375	15.9994	0.023902857	0.184908513	42.832314
N	0	0	14.0067	0	0	0
S	0	0	32.065	0	0	0
Cl	0	0	35.453	0	0	0
F	0	0	18.9984	0	0	0
Ash	4.1875	0.041875				4.69
H2O	10.71428571	0.107142857	18.0152	0.005947359	0.046007774	
Total	100	1	7.73583304	0.12926856	1	100

~ note: this total molar mass may be off, since "molar mass" of ash is not accounted for

Fuel "molecule"

a =	1.9697	
b =	0.713996	
MMfuel =	25.41947	kg/kmol
MC =	0.107143	
w =	0.177652	
Th. Air =	1.135427	mol O2/mol C

Input variables:

fuel rate:	0.062	kg/s
temperature:	1859	K
ambient T:	320	K

Syngas:

neglect NOx,SOx, Cl, F, tars, and ash.

	Moles/mole C	mole faction	MMgas	Mass flow rate (kg/s)	% wt. Comp.	HHV(kJ/kmol)	HHV(kJ/kg)	HHV (kJ/m3) at STP
H2	0.205618	3.8591	2.0158	0.0009	0.2873	285830.00	141794.82	11686.6751
CO	0.381025	7.1511	28.0101	0.0222	7.3988	282984.00	10102.93	11570.3113
CO2	0.618911	11.6157	44.0095	0.0565	18.8827	0.00	0.00	0
H2O(g)	0.956756	17.9564	18.0152	0.0358	11.9490	0.00	0.00	0
CH4	0.000064	0.0012	16.0423	0.0000	0.0007	890649.00	55518.78	36415.7908
N2	3.165836	59.4165	28.0134	0.1841	61.4815	0.00	0.00	0
Total	5.328211	100.0000		0.2994	100.0000	31277.43	1155.32	1278.83405

Air flow at inlet:

m =	0.8420	mol O2/mol C
% Th. Air =	74.1552	%
Inlet air flow:	0.2400	kg/s
	0.1959	m3/s

Mass Balance

	in	out
C	0.02493	0.02493
H	0.00486	0.00486
O	0.08553	0.08553
N2	0.18408	0.18408
Ash	0.00260	0.00260
Other	0.00000	0.00000
Total	0.30200	0.30200

	in	out
Air	0.24000	0.00000
Fuel	0.06200	0.00000
Syngas	0.00000	0.29940
Ash + trace	0.00000	0.00260
Total	0.30200	0.30200

Heat Balance:

Energy in (kW)		Energy out (kW)	
Air	0.00000	H2	20.32904065
Fuel	-342.4122806	CO	-47.15904315
Moisture	-105.39588	CO2	-400.2589793
		H2O(g)	-351.3858584
		CH4	0.004698083
		N2	330.6619815
Total	-447.8081605	Total	-447.8081605

Sheet 2: Properties

	A	B	C	D	E	F	G	H	I	J	K	L	M	N	O
1	**Specific Heat**														
2	from Zainal et al. 2001. He referenced Perry's Chemical Engineers' Handbook.														
3															
4		Cp = R*(A+B*Tam+C/3*(4*Tam^2-T1*T2)+D/(T1*T2))													
5															
6		**R =**	8.314	J/mol*K											
7		**T1 (amb.) =**	320	K											
8		**T2 (gas.) =**	1859	K											
9		**Tam =**	1089.5												
10															
11		Coefficients for Specific Heat relation:													
12	**gas**	**A**	**B**	**C**	**D**	**Cp (kJ/kmol*K)**	**HHV(kJ/kmol)**	**Hf°(kJ/kmol)**	**H(vap)**	**ΔH (kJ/kmol)**	**dHi at T2(kJ/kmol)**	**Gf°(kJ/kmol)**			
13	**CH4**	1.702	9.08E-03	-2.16E-06	0	71.50	890649.0	-74520.0		110038.3	35518.3	-50460			
14	**H2**	3.249	4.22E-04	0	8.30E+03	30.95	285830.0	0.0		47633.1	47633.1	0			
15	**CO**	3.376	5.57E-04	0	-3.10E+03	33.07	282984.0	-110525.0		50894.9	-59630.1	-137169			
16	**CO2**	5.457	1.05E-03	0	-1.16E+05	53.24		-393509.0		81930.7	-311578.3	-394359			
17	**N2**	3.28	5.93E-04	0	4.00E+03	32.70		0.0		50321.1	50321.1	0			
18	**O2**	6.085	2.02E-03	-5.28E-07	5.37E-11	62.79		0.0		96633.0	96633.0				
19	**H2O(g)**	3.47	1.45E-03	0	1.21E+04	42.15		-241818.0		64873.4	-176944.6	-228572			
20	**H2O(l)**							-285830.0	43998.5		-285830.0	-237129			
21	**C**	1.771	7.71E-04	0	-8.67E+04	20.50		0.0		31543.6		0			
22	**Fuel**						510039.2	-164969.5			-164969.5				
23															
24	**CH4 reaction ΔA = A(CH4) - A(C) - 2*A(H2) :**														
25		**ΔA1**	**ΔB1**	**ΔC1**	**ΔD1**			**ΔHf°1**			**ΔGf°1**	**J1 (298K)**	**I1 (298K)**	**ln(K1)**	**K1 (at T2)**
26		-6.567E+00	7.466E-03	-2.164E-06	7.010E+04			-7.452E+04			-5.046E+04	-5.821E+04	3.347E+01	-6.497E+00	0.00151
27															
28	**Shift rxn: ΔA = A(CO2) + A(H2) - A(CO) - A(H2O)**														
29		**ΔA2**	**ΔB2**	**ΔC2**	**ΔD2**			**ΔHf°2**			**ΔGf°2**	**J2 (298K)**	**I2 (298K)**	**ln(K2)**	**K2 (at T2)**
30		1.860E+00	-5.380E-04	0.000E+00	-1.164E+05			-4.117E+04			-2.862E+04	-4.891E+04	-1.770E+01	-1.052E+00	0.34909
31															
32		**Coefficients for Equation #3:**													
33		note: do not mix this up with A,B,C,D from Cp. Relation.													
34		**A =**	129974.074												
35		**B =**	-165226.595												
36		**C =**	-322571.099												
37		**D =**	108885.372												
38		**E =**	216529.543												
39															
40															
41															

Sheet 3: Solver

	A	B	C	D	E	F	G	H	I	J	K	L	M	N	O	P
1	**Solution Matrix**															
2																
3	$2x_1K_1$		1		1			Δx_1		$-(x_1^2K_1+x_2+x_3-1)$						
4	$-K_2x_2-x_3$		$-K_2x_1+(w+0.5a-2)K_2+4K_2x_2+2K_2x_3$		$-x_1+2K_2x_2$		X	Δx_2	=	$-[K_2x_1x_2+(w+0.5a-2)K_2x_2+2K_2x_2^2-x_1x_3+2K_2x_2x_3]$						
5	A		B		C			Δx_3		$-(Ax_1+Bx_2+Cx_3+Dw+E)$						
6																
7		0														
8				**w**	**a**	**K1**	**K2**	**A**	**B**	**C**	**D**	**E**	**X1***	**X2***	**X3***	**relax**
9				0.177652038	1.9697	0.001507	0.349088329	129.974	-165.2266	-322.5710992	108.8853717	216.5295426	0.5	0.5	0.5	
10																
11																
12																
13	**Iteration**	**1**														
14	**Coefficient Matrix:**				**Inverted matrix**				**B Matrix**		**Solution Matrix:**		**X1**	**X2**	**X3**	
15	0.0015073	1	1		1.052804	-0.78086	0.003629105		-0.000377		-0.31203515		0.187965	0.39593	0.604163	
16	-0.6745442	0.58036	-0.150911671		1.177175	0.647439	0.003346453		0.1343641		-0.104069723					
17	129.974074	-165.227	-322.5710992		-0.17876	-0.64626	-0.00335192		-56.96144		0.104163229					
18																
19	**Iteration**	**2**														
20	**Coefficient Matrix:**				**Inverted matrix**				**B Matrix**		**Solution Matrix:**		**X1**	**X2**	**X3**	
21	0.00058664	1	1		0.993217	-0.8479	0.00284653		-0.000147		0.017795547		0.20576	0.380909	0.619028	
22	-0.7423779	0.616694	0.088464427		1.228496	0.701391	0.004000804		-0.02116		-0.015021515					
23	129.974074	-165.227	-322.5710992		-0.22906	-0.70091	-0.00400242		0		0.014864672					
24																
25	**Iteration**	**3**														
26	**Coefficient Matrix:**				**Inverted matrix**				**B Matrix**		**Solution Matrix:**		**X1**	**X2**	**X3**	
27	0.00062028	1	1		0.973369	-0.83435	0.00286187		-4.77E-07		-0.000141939		0.205618	0.381025	0.618911	
28	-0.7519987	0.599885	0.060181209		1.244808	0.690271	0.0039878		0.0001696		0.00011645					
29	129.974074	-165.227	-322.5710992		-0.24541	-0.68975	-0.00398958		0		-0.00011684					
30																
31	**Iteration**	**4**														
32	**Coefficient Matrix:**				**Inverted matrix**				**B Matrix**		**Solution Matrix:**		**X1**	**X2**	**X3**	
33	0.00061986	1	1		0.973521	-0.83445	0.002861745		-3.04E-11		-9.0798E-09		0.205618	0.381025	0.618911	
34	-0.7519225	0.600015	0.060404451		1.244683	0.690358	0.003987906		1.085E-08		7.44963E-09					
35	129.974074	-165.227	-322.5710992		-0.24529	-0.68984	-0.00398968		0		-7.47437E-09					
36																
37	**Iteration**	**5**														
38	**Coefficient Matrix:**				**Inverted matrix**				**B Matrix**		**Solution Matrix:**		**X1**	**X2**	**X3**	
39	0.00061986	1	1		0.973521	-0.83445	0.002861745		1.11E-16		8.49218E-17		0.205618	0.381025	0.618911	
40	-0.7519225	0.600015	0.060404465		1.244683	0.690358	0.003987906		2.776E-17		1.57349E-16					
41	129.974074	-165.227	-322.5710992		-0.24529	-0.68984	-0.00398968		0		-4.63792E-17					
42																

Sheet 4: Stoichiometric Calculations

	A	B	C	D	E	F	G	H	I	J	K	L	M	N
1	**Stoichiometric Calculations**													
2														
3	**Assumptions:**													
4	1. Both fuel composition and flue gas composition are known.													
5	2. Adiabatic													
6	3. Sub-stoichiometric, stoichiometric, or excess air may be used.													
7														
8	all user inputs are in blue		important outputs are in orange											
9														
10	**Input**													
11		**Fuel rate**	0.062	kg/s (wet)		**O2 supply**	99.06996598	% substoichiometric						
12		**Air flow**	0.00301	kg/s										
13		**Temp in**	320	K		**Fuel rate (dry)**	0.055357143	kg/s						
14		**Char conversion**	100	%		**Fuel rate (converted)**	0.055357143	kg/s						
15						**Fuel rate**	0.002075609	mol/s						
16	**Fuel Composition**					**Air flow**	2.19181E-05	mol/s						
17						**Th. Air**	0.323644074	kg/s						
18	**Proximate Analyisis**					**O2 supply**	0.010559857	mol O2 / mol C				**Fuel Molecule - CHaOb + wH2O**		
19		**Moisture**	12	%							**a**	1.969700047		
20		**Volatiles**	79.28	%							**b**	0.713996164		
21		**Fixed Carbon**	16.03	%							**w**	0.177652038		
22		**Ash**	4.69	%							**MMfuel**	25.4194709	kg/kmol	
23														
24	**Ultimate Analysis**											**Th. Air**	1.13542693	mol O2/mol C
25			**% mass (dry)**	**% mass (converte**	**% mass (wet)**	**mass fraction (mfi)**	**Molar Mass**	**mfi/Mi**	**mole fraction**	**dry %mass**				
26		**C**	47.25	47.25	40.20890625	0.402089063	12.0107	0.033477571	0.2589769	40.20891				
27		**H**	7.81	7.81	6.646170536	0.066461705	1.0079	0.065940773	0.510106812	6.646171				
28		**O**	44.94	44.94	38.2431375	0.382431375	15.9994	0.023902857	0.184908513	38.24314				
29		**N**	0	0	0	0	14.0067	0	0	0				
30		**S**	0	0	0	0	32.065	0	0	0				
31		**Cl**	0	0	0	0	35.453	0	0	0				
32		**F**	0	0	0	0	18.9984	0	0	0				
33		**Ash**			4.1875	0.041875				4.1875				
34		**H2O**			10.71428571	0.107142857	18.0152	0.005947359	0.046007774					
35		**Total**	100	100	100	1	7.73583304	0.12926856	1	89.28571				
36														
37	**Gas Composition**													
38			**% mass**	**mol / mol C**	**Molar Mass**	**Mass Flow Rate (kg/s)**	**Mol fraction**	**%mass (gases only)**		**3D**	**Error**	**Er^Er**		
39		**H2**	5.020043811	0.78	2.0158	0.00326353	0.389570085	5.228864603		0.331684	-4.89718	23.98237811		
40		**CO**	95.66564014	1.069734146	28.0101	0.062192233	0.534277465	99.64508246		20.55214	-79.0929	6255.692894		
41		**CO2**	-23.84960104	-0.169734146	44.0095	-0.015504626	-0.08477352	-24.84168254		6.847853	31.68954	1004.22668		
42		**H2O(g)**	10.49717233	0.182502062	18.0152	0.006824212	0.091150441	10.93382746		13.72299	2.789164	7.779434771		
43		**CH4**	5.121911821	0.1	16.0423	0.003329755	0.049944883	5.334970059		0.105198	-5.22977	27.35051422		
44		**N2**	3.551216562	0.039705061	28.0134	0.002308646	0.019830646	3.698937954		56.31457	52.61563	2768.404442		
45		**O2**	0	0	31.9988	0	0	0		2.125562	2.125562	4.518013737		
46		**Ash**	3.993616367			0.00259625	0							
47		**Total**	100	2.002207123		0.06501	1	100		100				
48														
49										RMS error:	37.96983			

	A	B	C	D	E	F	G	H
49								
50	**Heat Balance**							
51								
52			**Mass in (kg/s**	**Mass out (kg/s)**	**Hf0 (kJ/kmol)**	**Chem. Heat in (kW)**	**Chem. Heat out (kW)**	
53		**Fuel**	0.055357143	0	-164969.5168	-359.261652	0	
54		**H2O(l)**	0.006642857	0	-285830	-105.39588	0	
55		**H2**	0	0.00326353	0	0	0	
56		**CO**	0	0.062192233	-110525	0	-245.4042119	
57		**CO2**	0	-0.015504626	-393509	0	138.6339251	
58		**H2O(g)**	0	0.006824212	-241818	0	-91.6013829	
59		**CH4**	0	0.003329755	-74520	0	-15.46744128	
60		**N2**	0.002308646	0.002308646	0	0	0	
61		**O2**	0.000701354	0	0	0	0	
62		**Ash**	0	0.00259625	0	0	0	
63		**Unburnt Char**	0	0	0	0	0	
64		**Total**	0.06501	0.06501		-464.657532	-213.8391109	
65								
66								
67		**Temp in (K)**	320	K				
68		**Cp (gas)**	1.310066917	kJ/kmol*K				
69		**dH(rxn)**	-250.8184211	kW				
70		**Temp out (K)**	-2625.00329	K				
71								
72								
73								
74		Cp slope	0.000182021					
75		Cp y-int	1.787873552					
76		A =	1.18332E-05					
77		B =	0.112443033					
78		C =	213.6249301					
79		Temp out (K)	-2625.00329					
80								
81	**Volatiles and Char Breakdown**							
82	* Note: Char Conversion MUST be set to 100% for these calculations to be valid!!							
83								
84		CHaOb => mC(s) + nCHxOy(g)						
85								
86		mol fraction of C(dry) =	0.271466468					
87		Moles C to char =	0.096629433					
88		Moles C to vols =	0.174837035					
89								
90		a =	1.969700047		m =	0.355953477		
91		b =	0.713996164		n =	0.644046523		
92					x =	3.058319512		
93					y =	1.108609609		
94					MM(vols) =	32.83026882		
95								
96		**Species**	**Stoich. Coeff**	**HHV (kJ/kmol)**	**dH**			
97		CHaOb (dry fuel)	1	510039.17	510039.17			
98		C(s)	0.355953477	393509.00	140070.90			
99		CHxOy(gas)	0.644046523	574443.39	369968.27			
100								
101		**dH of Rxn:**	0.00	kJ/kmol C				

	A	B	C	D	E	F	G
103	**Volatiles Decomposition**						
104							
105							
106		CHxOy => aCO + bCO2 + cCH4 + dH2					
107							
108		x =	3.058319512		b =	0.204304805	
109		y =	1.108609609		c =	0.095695195	
110		a =	0.7		d =	1.337769365	
111							
112							
113		**Species**	**Stoich. Coeff**	**Hf0 (kJ/kmol)**	**dH**		
114		CHxOy	1	-256145.34	-256145.34		
115		CO	0.7	-110525.00	-77367.50		
116		CO2	0.204304805	-393509.00	-80395.78		
117		CH4	0.095695195	-74520.00	-7131.21		
118		H2	1.337769365	0.00	0.00		
119							
120		**dH of Rxn:**	-91250.86	kJ/kmol C			
121							
122	**Char Combustion**						
123							
124							
125		C(s) + 0.5O2 => CO					
126							
127		**Species**	**Stoich. Coeff**	**Hf0 (kJ/kmol)**	**dH**		
128		C(s)	1	0.00	0.00		
129		O2	0.5	0	0.00		
130		CO	1	-110525.00	-110525.00		
131							
132		**dH of Rxn:**	110525.00	kJ/kmol C			
133							
134	**Volatiles Overall Combustion (Complete, H2O => Liquid!)**						
135							
136							
137		CHxOy + mO2 => aCO2 + bH2O(l)					
138							
139		x =	3.058319512		a =	1	
140		y =	1.108609609		b =	1.529159756	
141		m =	1.764579878				
142							
143							
144		**Species**	**Stoich. Coeff**	**Hf0 (kJ/kmol)**	**dH**		
145		CHxOy(g)	1	-256145.34	-256145.34		
146		O2	1.764579878	0	0.00		
147		CO2	1	-393509.00	-393509.00		
148		H2O(l)	1.529159756	-285830.00	-437079.73		
149							
150		**dH of Rxn:**	574443.39	kJ/kmol C			
151							
152	**Char Combustion (Complete)**						
153							
154		C(s) + O2 => CO2					
155							
156		**Species**	**Stoich. Coeff**	**Hf0 (kJ/kmol)**	**dH**		
157		C(s)	1	0.00	0.00		
158		O2	1	0	0.00		
159		CO2	1	-393509.00	-393509.00		
160							
161		**dH of Rxn:**	393509.00	kJ/kmol C			
162							
163							

Appendix C: Fluent Parameter List

Vidir Arborg Gasifier
FLUENT Parameters

Grid Menu

Scale Grid		
Grid was created in	in	
X scale factor	0.0254	
Y scale factor	0.0254	
Z scale factor	0.0254	
Xmin	-5.08	m
Ymin	-0.254	m
Zmin	-0.55537	m
Xmax	0.555371	m
Ymax	2.786634	m
Zmax	0.707771	m

Models

Solver	
Solver	Segregated
Space	3D
Velocity Formulation	Absolute
Gradient Option	Cell-based
Formulation	Implicit
Time	Steady
Porous Formulation	Superficial Velocity

Multiphase Model	
Model	Off

Energy	
Energy Equation	On

Viscous Model	
Model	k-epsilon
k-epsilon Model	Standard

Species Model	
Model	Species Transport
Reactions	Volumetric
Inlet Diffusion	On
Diffusion Energy Source	On
Full Multicpnt Diff	Off
Thermal Diffusion	Off
Mixture Material	straw-volatiles-air
Number of Vol. Species	8
Turb-Chem Interaction	Eddy-Dissipation

Discrete Phase Model	
Interaction with Cont. Phase	On
Update DPM sources every iter	Off
Num Cont. Phase Iter. Per DPM Iter	200
Unsteady Particle Tracking	Off
Max. Number of Steps	2000
Step Length Factor	10

	Standard
Near-Wall Treatment	Wall Fcns
Viscous Heating	Off
Cmu	0.09
C1-Epsilon	1.44
C2-Epsilon	1.92
TKE Prandtl Number	1
TDR Prandtl Number	1.3
Energy Prandtl Number	0.85
Wall Prandtl Number	0.85
Turb. Schmidt Number	0.7
UDFs	None

Radiation	
Model	P1
Solar Load	Off

	udf
Drag Law	particle_drag_force
Physical models	all off
UDF Body Force	particle_body_force
Scalar Update	none
Source	none
DPM Time Step	none
Number of Scalars	0
Accuracy Control	On
Tolerance	1.00E-05
Max Refinements	20
Automated tracking scheme selection	On
High Order Scheme	trapezoidal
Low Order Scheme	implicit
Coupled Heat-Mass Solution	Off

Boundary Conditions and Operating Conditions

Operating Conditions			
Operating Pressure		101325	Pa
Ref P Location X		0	m
Ref P Location Y		0	m
Ref P Location Z		0	m
Gravity	On		
Grav. Accel. X		0	m/s^2
Grav. Accel. Y		-9.81	m/s^2
Grav. Accel. Z		0	m/s^2
Bous. Operating Temp		288.16	K
Specific Operating Density	Off		

Boundary Condition 1	
Zone Name	air
Type	Fluid
Source Terms	Off
Fixed Values	Off
Porous Zone	Off
Laminar Zone	Off
Reaction	On

Motion Type	Stationary	
Reaction Mechanism	mechanism-1	

Boundary Condition 2		
Zone Name	air_inlet	
Type	mass-flow-inlet	
Mass Flow Spec. method	Mass Flow Rate	
Mass Flow Rate	0.1	kg/s
Total Temperature	320	K
Supersonic/Init Guage P	0	Pa
Direction Spec. Method	Normal to Boundary	
Reference Frame	Absolute	
Turbulence Spec. Method	Intensity and H. Diam	
Turbulence Intensity	10	%
Hydraulic Diameter	0.060325	m
O2 Mass Fraction	0.23	
CO2 Mass Fraction	0	
H2O Mass Fraction	0	
straw_vol Mass Fraction	0	
CH4 Mass Fraction	0	
CO Mass Fraction	0	
H2 Mass Fraction	0	
Ext. Black Body Temp Method	Boundary Temperature	
Internal Emissivity	1	
Discrete Phase BC Type	escape	

Boundary Condition 3	
Zone Name	default-interior
Type	interior

Boundary Condition 4	
Zone Name	default-interior:008
Type	interior

Boundary Condition 5	
Zone Name	default-interior:010
Type	interior

Boundary Condition 6		
Zone Name	fuel_in	
Type	mass-flow-inlet	
Mass Flow Spec. method	Mass Flow Rate	
Mass Flow Rate	0.06	kg/s
Total Temperature	320	K
Supersonic/Init Guage P	0	Pa

Direction Spec. Method	Normal to Boundary	
Reference Frame	Absolute	
Turbulence Spec. Method	Intensity and H. Diam	
Turbulence Intensity	10	%
Hydraulic Diameter	0.3307	m
O2 Mass Fraction	0.23	
CO2 Mass Fraction	0	
H2O Mass Fraction	0	
straw_vol Mass Fraction	0	
CH4 Mass Fraction	0	
CO Mass Fraction	0	
H2 Mass Fraction	0	
Ext. Black Body Temp Method	Boundary Temperature	
Internal Emissivity	1	
Discrete Phase BC Type	escape	

Boundary Condition 7		
Zone Name	fuelbed	
Type	Fluid	
Source Terms	Off	
Fixed Values	Off	
Porous Zone	On	
Laminar Zone	Off	
Reaction	On	
Motion Type	Stationary	
Reaction Mechanism	mechanism-1	
Direction-1 Vector X	1	
Direction-1 Vector Y	0	
Direction-1 Vector Z	0	
Direction-1 Vector X	0	
Direction-1 Vector Y	1	
Direction-1 Vector Z	0	
Viscous R Direction-1	0	1/m^2
Viscous R Direction-2	0	1/m^2
Viscous R Direction-3	0	1/m^2
Internal R Direction-1		1/m
Internal R Direction-2		1/m
Internal R Direction-3		1/m
Power Law Model C0	0	
Power Law Model C1	0	
Fluid Porosity	udf porosity_lin_profile	
Solid Material Name	straw	

Boundary Condition 8	
Zone Name	outlet
Type	outflow
Flow Rate Weighting	1
Ext. Black Body Temp	Boundary Temperature

Method		
Internal Emissivity	1	
Discrete Phase BC Type	escape	

Boundary Condition 9		
Zone Name	wall	
Type	wall	
Adjacent Cell zone	air	
Thermal Conditions	Heat Flux	
Heat Flux	0	W/m^2
Internal Emissivity	0.5	
Wall Thickness	0	m
Heat Generation Rate	0	W/m^3
Material Name	calcium-sulfate	

Boundary Condition 10		
Zone Name	wall:001	
Type	wall	
Adjacent Cell zone	fuelbed	
Thermal Conditions	Heat Flux	
Heat Flux	0	W/m^2
Internal Emissivity	0.5	
Wall Thickness	0	m
Heat Generation Rate	0	W/m^3
Material Name	calcium-sulfate	

Species Transport and Reaction

Material Properties of Straw-volatiles-air

Mixture Species	
Species 1	O2
Species 2	CO2
Species 3	H2O
Species 4	straw_vol
Species 5	CH4
Species 6	CO
Species 7	H2
Species 8	N2

Reactions		
Mixture	straw-volatiles-air	
Tot. Num. of Reactions		5
1: Reaction Type	Volumetric	
1: Number of Reactants		1
1: Number of Products		4
1: Mixing Rate, A		4
1: Mixing Rate, B		0.5
2: Reaction Type	Volumetric	
2: Number of Reactants		3
2: Number of Products		2
2: Mixing Rate, A		4
2: Mixing Rate, B		0.5
3: Reaction Type	Volumetric	
3: Number of Reactants		2
3: Number of Products		2
3: Mixing Rate, A		4
3: Mixing Rate, B		0.5
4: Reaction Type	Volumetric	
4: Number of Reactants		2
4: Number of Products		1
4: Mixing Rate, A		4
4: Mixing Rate, B		0.5
5: Reaction Type	Volumetric	
5: Number of Reactants		2
5: Number of Products		2
5: Mixing Rate, A		4
5: Mixing Rate, B		0.5

Mechanism	
Number of Mechanisms	1
Mechanism ID	1
Name	mechanism-1
Reaction Type	Volumetric
Reactions	reaction-1
	reaction-2
	reaction-3
	reaction-4
	reaction-5

Reaction 1

Species	Reactant/Product	Stoich. Coefficient	Rate Exponent
straw_vol	Reactant	1	1
CO	Product	0.6	0
CO2	Product	0.254	0

CH4	Product	0.146	0
H2	Product	1.238	0

Reaction 2

Species	Reactant/Product	Stoich. Coefficient	Rate Exponent
CO	Reactant	1	1
O2	Reactant	0.5	0.25
H2O	Reactant	1	0.5
CO2	Product	1	0
H2O	Product	1	0

Reaction 3

Species	Reactant/Product	Stoich. Coefficient	Rate Exponent
CH4	Reactant	1	0.7
O2	Reactant	1.5	0.8
CO	Product	1	0
H2O	Product	2	0

Reaction 4

Species	Reactant/Product	Stoich. Coefficient	Rate Exponent
H2	Reactant	1	1.5
O2	Reactant	0.5	1
H2O	Product	1	0

Reaction 5

Species	Reactant/Product	Stoich. Coefficient	Rate Exponent
H2O	Reactant	1	1
CO	Reactant	1	1
H2	Product	1	1
CO2	Product	1	1

Properties of straw-volatiles-air

Density	incompressible-ideal-gas	
Cp	mixing law	J/kg*K
Thermal Conductivity	0.0454	W/m*K
Viscosity	1.72E-05	kg/m*s
Mass Diffusivity	2.88E-05	m^2/s
Absorption Coefficient	0	1/m
Scattering Coefficient	0	1/m
Scattering Phase Function	isotropic	

Materials

straw-volatiles-air		
Material Type	mixture	
Density	incompressible-ideal-gas	
Cp	mixing law	J/kg*K
Thermal Conductivity	0.0454	W/m*K
Viscosity	1.72E-05	kg/m*s
Mass Diffusivity	2.88E-05	m^2/s
Absorption Coefficient	0	1/m
Scattering Coefficient	0	1/m
Scattering Phase Function	isotropic	

CH4		
Material Type	fluid	
Mixture	straw-volatiles-air	
Cp	piecewise-polynomial	J/kg*K
Molecular Weight	16.04276	kg/kmol
Standard State Enthalpy	-7.49E+07	J/kmol
Standard State Entropy	186043.9	J/kmol
Reference Temperature	298	K

CO		
Material Type	fluid	
Mixture	straw-volatiles-air	
Cp	piecewise-polynomial	J/kg*K
Molecular Weight	28.0104	kg/kmol
Standard State Enthalpy	-1.11E+08	J/kmol
Standard State Entropy	197535.7	J/kmol
Reference Temperature	298	K

CO2		
Material Type	fluid	
Mixture	straw-volatiles-air	
Cp	piecewise-polynomial	J/kg*K
Molecular Weight	44.0098	kg/kmol
Standard State Enthalpy	-3.94E+08	J/kmol
Standard State Entropy	213720.2	J/kmol
Reference Temperature	298	K

H2		
Material Type	fluid	
Mixture	straw-volatiles-air	
Cp	piecewise-polynomial	J/kg*K
Molecular Weight	2.01588	kg/kmol
Standard State Enthalpy	-1882.081	J/kmol
Standard State Entropy	130581.7	J/kmol
Reference Temperature	298	K

H2O		
Material Type	fluid	
Mixture	straw-volatiles-air	
Cp	piecewise-polynomial	J/kg*K
Molecular Weight	18.01528	kg/kmol
Standard State Enthalpy	-2.42E+08	J/kmol
Standard State Entropy	188700.3	J/kmol
Reference Temperature	298	K

N2		
Material Type	fluid	
Mixture	straw-volatiles-air	
Cp	piecewise-polynomial	J/kg*K
Molecular Weight	28.0134	kg/kmol
Standard State Enthalpy	-2930.741	J/kmol
Standard State Entropy	191498.7	J/kmol
Reference Temperature	298	K
O2		
Material Type	fluid	
Mixture	straw-volatiles-air	
Cp	piecewise-polynomial	J/kg*K
Molecular Weight	31.9988	kg/kmol
Standard State Enthalpy	-5244.882	J/kmol
Standard State Entropy	205031.1	J/kmol
Reference Temperature	298	K
straw-volatiles		
Material Type	fluid	
Mixture	straw-volatiles-air	
Cp	1500	J/kg*K
Molecular Weight	32.83027	kg/kmol
Standard State Enthalpy	-32443550	J/kmol
Standard State Entropy	0	J/kmol
Reference Temperature	298.15	K
calcium-sulfate		
Material Type	solid	
Density	2960	kg/m^3
Cp	856	J/kg*K
Thermal Conductivity	0.5	W/m*K
straw		
Material Type	solid	
Density	410	kg/m^3
Cp	0	J/kg*K

Thermal Conductivity	0.05	W/m*K

straw-particles		
Material Type	combusting-particle	
Density	410	kg/m^3
Cp	1250	J/kg*K
Thermal Conductivity	0.05	W/m*K
Latent Heat	0	J/kg*K
Vaporization Temperature	400	kg/m^3
Volatile Comp. Fraction	79.28	%
Binary Diffusivity	4.00E-05	m^2/s
Swelling Coefficient	1	
Burnout Stoichiometric Ratio	1.333	
Combustible Fraction	16.03	%
Heat of Rxn for Burnout	9202211	J/kg
Rxn. Heat Frac. Absorbed by Solid	0	%
Devolatilization Model	single rate	1/s
Combustion Model	diffusion-limited	

Injections

injection-0	
Injection Type	file
Particle Type	Combusting
Custom Laws	off
Material	straw-particles
Oxidizing Species	O2
Evaporating Species	H2O
Devolatilizing Species	straw-vol
Product Species	CO
Point Properties	NA
Discrete Random Walk	Off
Random Eddy Lifetime	Off
Cloud Model	Off
Wet Combustion Model	On
Liquid Material	water-liquid
Liquid Fraction	0.046938
Initialization UDF	none
Multiple Reactions	NA

Solver

Solution Controls	
Pressure-Velocity Coupling	SIMPLEC
Skewness Correction	0
Pressure URF	0.04
Density URF	0.04
Body Force URF	0.04
Momentum URF	0.04
Turbulent Kinetic Energy URF	0.1
Turbulent Dissipation Rate URF	0.1
Turbulent Viscosity URF	0.1
O2 URF	0.08
CO2 URF	0.08
H2O URF	0.08
straw_vol URF	0.08
CH4 URF	0.08
CO URF	0.08
H2 URF	0.08
Energy URF	0.1
P1 URF	0.1
Discrete Phase Sources URF	0.1
Pressure Discretization	Standard
Density Discretization	First Order Upwind
Body Force Discretization	First Order Upwind
Momentum Discretization	First Order Upwind
Turbulent Kinetic Energy Discretization	First Order Upwind
Turbulent Dissipation Rate Discretization	First Order Upwind
Turbulent Viscosity Discretization	First Order Upwind
O2 Discretization	First Order Upwind
CO2 Discretization	First Order Upwind
H2O Discretization	First Order Upwind
straw_vol Discretization	First Order Upwind
CH4 Discretization	First Order Upwind
CO Discretization	First Order Upwind
H2 Discretization	First Order Upwind
Energy Discretization	First Order Upwind
P1 Discretization	First Order Upwind
Discrete Phase Sources Discretization	First Order Upwind

*** Create a temperature patch to the temperature predicted by equilibrium model.**

Solution Initialization		
Gauge Pressure	0	Pa
X Velocity	0	m/s
Y Velocity	0	m/s
Z Velocity	0	m/s

Turbulece Kinetic Energy	0.1	m^2/s^2
Turbulence Dissipation Rate	0.1	m^2/s^2
O2	0.1	
CO2	0	
H2O	0	
straw_vol	0	
CH4	0.03	
CO	0.1	
H2	0	
Temperature*	320	K

Residual Monitors	
Continuity	0.001
x-velocity	0.0001
y-velocity	0.0001
z-velocity	0.0001
energy	1.00E-05
k	0.0001
epsilon	0.0001
O2	0.0001
CO2	0.0001
CO2	0.0001
H2O	0.0001
straw_vol	0.0001
CH4	0.0001
CO	0.0001
H2	0.0001
P1	1.00E-06